Investigation of Mpemba Effect in Two-dimensional q-state Potts model

A Thesis

Submitted in partial fulfilment for the degree of

MASTER OF SCIENCE

as a part of Integrated Ph.D. programme

(Materials Science)

by

Sohini Chatterjee

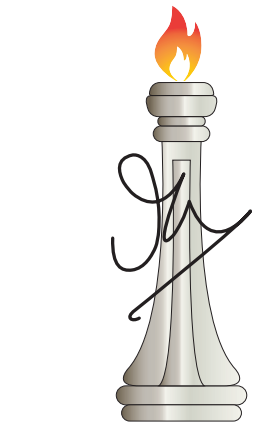

THEORETICAL SCIENCES UNIT
JAWAHARLAL NEHRU CENTRE FOR ADVANCED SCIENTIFIC RESEARCH
(A Deemed University)
Bangalore – 560 064

April 2022

To my late grandmothers

DECLARATION

I hereby declare that the matter embodied in the thesis entitled "**Investigation of Mpemba Effect in Two-dimensional q-state Potts model**" is the result of investigations carried out by me at the Theoretical Sciences Unit, Jawaharlal Nehru Centre for Advanced Scientific Research, Bangalore, India under the supervision of **Prof. Subir K. Das**, and that it has not been submitted elsewhere for the award of any degree or diploma.

In keeping with the general practice in reporting scientific observations, due acknowledgment has been made whenever the work described is based on the findings of other investigators.

Sohini Chatterjee

CERTIFICATE

I hereby certify that the matter embodied in this thesis entitled "**Investigation of Mpemba Effect in Two-dimensional q-state Potts model**" has been carried out by **Sohini Chatterjee** at the Theoretical Sciences Unit, Jawaharlal Nehru Centre for Advanced Scientific Research, Bangalore, India under my supervision and that it has not been submitted elsewhere for the award of any degree or diploma.

Prof. Subir K. Das

(Research Supervisor)

Acknowledgements

I owe my deepest gratitude to my supervisor, Prof. Subir K. Das, for his constant support and guidance. I am thankful to him for introducing me to a very exciting and interesting problem for my MS project, which I really enjoyed working on. His encouraging words and feedback have helped me to move forward with this project. This dissertation would not have been possible without his fruitful advises and suggestions.

I sincerely extend my gratitude to the CPMU Chair, Prof. A. Sundaresan, and Integrated Ph.D. coordinators, earlier, Prof. Kavita Jain and Prof. Rajesh Ganapathy, and present, Prof. Shobhana Narasimhan and Prof. Ranjan Dutta, for giving me the opportunity to explore the field of my interest. I thank all my course instructors, Prof. Aloknath Chakrabarti, Prof. A. Sundaresan, Prof. Balasubramanian, Dr. Bivas Saha, Prof. Chandrabhas Narayana, Dr. Diwakar Venkatesan, Prof. Eswaramoorthy, Prof. Kavita Jain, Prof. Meheboob Alam, Prof. Narayan K.S., Dr. Premkumar Senguttuvan, Prof. Rajesh Ganapathy, Prof. Ranjan Datta, Dr. Sarit Agasti, Prof. Shobhana Narasimhan, Dr. Sridhar Rajaram, Prof. Subir K. Das, Prof. Umesh V. Waghmare, Prof. Vidhyadhiraja N.S., from whose teachings I have benefited. I really enjoyed attending all the courses and learnt a lot from them.

Thanks to all my lab mates, Dr. Nalina, Koyel, Arabinda, Soumik, Dr. Tanay, Purnendu, Anjaney, for all the helpful discussions. Particular thanks to Dr. Nalina for her kind and friendly suggestions.

I acknowledge Paramyukti National Supercomputing facility (NSM) at JNCASR, using which I carried out the computational work of this thesis.

I am thankful to JNCASR for financial support. I am grateful to all the authorities in JNCASR - administrative, academic, library, technical, hostel and support staff, whose efforts have helped in making my stay in JNCASR very comfortable.

I am indebted to my parents for all their selfless sacrifices and priceless efforts. There are not enough words in the dictionary to thank them. Special thanks to my loving sister, Sarbani, for all her helpful scientific and non-scientific suggestions.

Synopsis

One may put a hot and a relatively colder glass of water simultaneously inside a refrigerator and expect the colder one to freeze faster. But it is observed that the hotter water freezes earlier. This counter-intuitive phenomenon, known as the 'Mpemba effect', has been an important subject of discussion in the past decade. Earlier this effect was thought to be true only for liquid systems, but, recently, the effect has been seen to be present in a variety of other systems. In the literature, nevertheless, there exists experimental evidences in favour as well as against the existence of this effect, even in the case of water. This thesis contains results and discussion based on our investigation of this puzzling effect in the context of the para-to-ferromagnetic transitions in the two-dimensional generalised Ising model, i.e., the 'q-state Potts model'.

The thesis is divided into three chapters. In **chapters** 1 and 2, we create a theoretical background, introducing the concepts and techniques. In **chapter** 3 we discuss the results.

Chapter 1 starts with a brief introduction to phase transitions and critical phenomena. We discuss the important theories of phase ordering dynamics. In this chapter we provide all the necessary information related to the Potts model. We have also provided our motivation and a brief overview of the thesis.

In **Chapter** 2, we discuss in detail about the computational techniques and protocol followed to carry out the simulations. We further describe and provide details of the methodologies required to analyse the simulation results.

We present the results of our observation in **Chapter** 3. We prepare systems at different starting temperatures, T_s, above the critical temperature T_c, and quench them to low temperatures, viz., $T_l = 0$ and $0.5\,T_c$. We perform this protocol for a set of q values of the q-state Potts model. Interestingly, we observe Mpemba effect to exist in second-order, weakly first-order and first-order phase transitions of the model, in the case of quench to $T_l = 0.5\,T_c$. Strikingly, the effect is not so strong when the systems are quenched to $T_l = 0$. We briefly discuss possible reasons of the nonparallel observations in the non-zero and zero temperature quench cases. Our observation suggests that the effect gets weaker with the increase of q.

Publications

"Observation of Mpemba Effect in Potts Model and Long-range Ising Model", Sohini Chatterjee, Soumik Ghosh, Nalina Vadakkayil, and Subir K. Das, Manuscript under preparation.

Table of contents

List of figures

List of tables

Chapter 1

Introduction

1.1 Phase Transition: A general overview

The study of phase transitions is of fundamental importance. Phase transition occurs in a system when it is subjected to variations in thermodynamic parameters [1–7] such as pressure (P), temperature (T), density (ρ) and magnetic field (H). This commonly observed phenomena finds large industrial applications. An important example of phase transition is that of water, which can exist in either of solid, liquid or vapor phases.

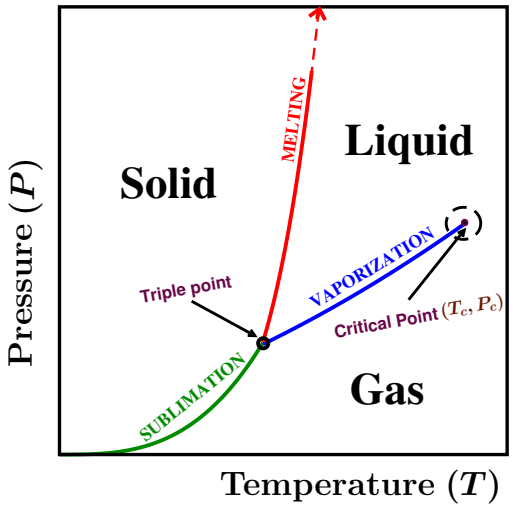

Figure 1.1: Schematic diagram showing phases of a normal chemical substance in P - T plane. The solid lines are the coexistence curves across which first-order phase transitions occur.

The schematic in Fig. 1.1 shows the phase diagram of a chemical substance in P - T plane [2, 7]. At any particular T and P, the phase with the lowest Gibbs energy

[1, 7], $G(T, P)$, will exist. The three distinct phases, namely, solid, liquid and gas, are separated from each other by the phase boundaries, referred to as the coexistence curves. Along these curves, two different phases coexist in equilibrium. For example, the solid and liquid phases coexist along the fusion or melting curve; solid and gas along the sublimation curve; and the liquid and gaseous phases coexist along the vaporization curve [1, 2]. While crossing these curved lines a system encounters discontinuity in densities (first-order derivative of Gibbs free energy), resulting in first-order phase transitions [1, 2].

All the three phases coexist in equilibrium at the triple point. It can be seen from the diagram that, although the melting curve is never ending, the vaporization curve terminates at a point called the critical point [1, 2, 7], denoted by the coordinates (T_c, P_c), T_c being the critical temperature and P_c, the critical pressure. Beyond this point, there is no difference between the liquid and gaseous phases and one can readily convert a liquid to a gas, or vice versa, continuously, without crossing the vaporization curve [1, 2]. Here, although the densities of the phases become continuous, certain second-order derivatives of the free energy is singular. Such a phase transition is referred to as a continuous or second-order phase transition [1, 2, 7].

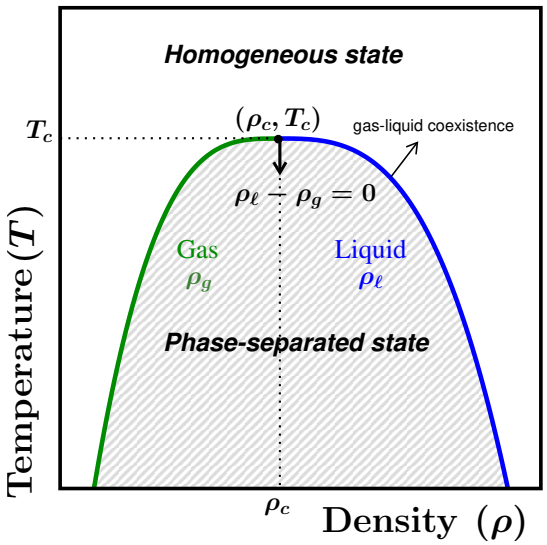

Figure 1.2: Schematic coexistence curve of a liquid-gas system in the ρ - T plane. Here, ρ_c denotes the critical density and T_c the critical temperature. The left and right branches of the coexistence curve correspond to the vapor and liquid phases, respectively.

Phase transitions are marked by the variation in a quantity called the order parameter [3–10], ψ. When a phase changes, this quantity undergoes a variation from one value to the other, depicting a transition. For a phase transition between liquid and gaseous phases,

the order parameter can be defined as [2–5] $\psi = \rho_\ell - \rho_g$, where ρ_ℓ is the density in the liquid phase and ρ_g is the density in the gaseous phase. In Fig. 1.2, the coexistence curve of a liquid-gas transition in the vicinity of the critical point has been shown schematically in the ρ - T plane. In this phase diagram, the system is in a homogeneous phase with a uniform spatial density outside the shaded region. Whereas, inside the shaded region, the system exists in a two-phase state each having different density from the other. It is evident from the diagram that the left and right branches of the coexistence curve, corresponding to the low density gaseous and high density liquid phases, respectively, are approaching each other with the increase in temperature. This implies that the density difference between the liquid and gaseous phases, i.e., the order parameter, goes on decreasing continuously with rise in temperature, until, it finally becomes zero at T_c.

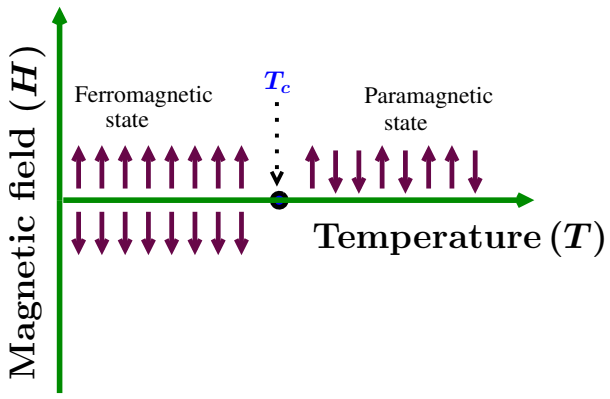

Figure 1.3: Schematic phase diagram of a magnetic system, with para-to-ferromagnetic transition, in the H - T plane. Here T_c is the *Curie temperature*, denoting a second-order critical point. Below T_c, the system can acquire either all up or all down spins.

Another common and important example of phase transition is the para-to-ferro transition in magnetic systems [7, 10]. The phase diagram of such a transition is shown in Fig. 1.3 in the H - T plane, H being the external magnetic field. For such transitions, with $H = 0$, T_c is known as the *Curie temperature*. Above T_c, the system is in a disordered state, referred to as the paramagnetic state, with randomly oriented spins, providing zero net magnetisation to the system. Below T_c, majority of the spins align in a particular direction. The parallel orientation of the spins results in a net non-zero magnetization of the system. Hence, for such systems, the correct choice of order parameter (ψ) is the magnetisation. The phase diagram of the above mentioned system in the m - T plane at $H = 0$ can be viewed in Fig. 1.4. A system at temperature T_s ($> T_c$) exists in equilibrium in a paramagnetic phase. At temperature T_l ($< T_c$) there are two possible

equilibrium phases with magnetisation $\pm m_o$, depending on the orientation of the spins, in a uniaxial magnet.

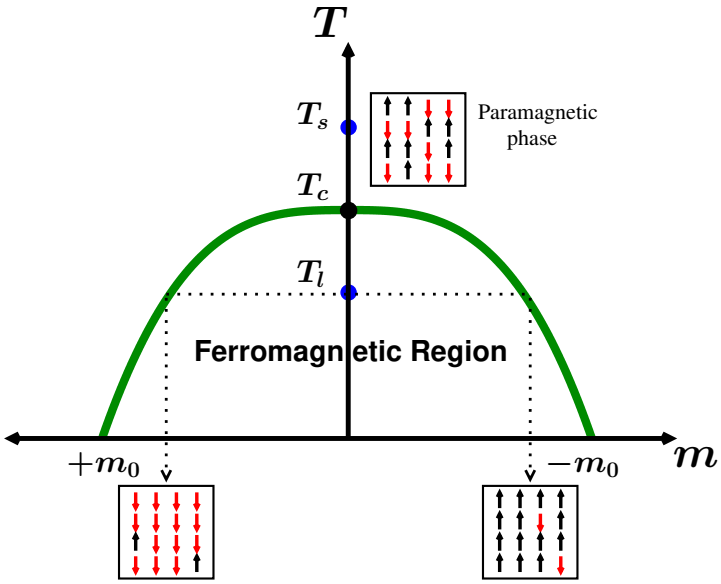

Figure 1.4: Schematic phase diagram of a magnetic system exhibiting para-to-ferromagnetic transition in the m - T plane with $H = 0$.

Note here that when the thermodynamic parameters, temperature, pressure, etc., are suddenly changed, the homogeneous systems are rendered thermodynamically unstable and are put into far-from-equilibrium states [7, 10]. Let us consider the rapid quench to temperatures below the critical point. The systems cannot reach the new equilibrium state immediately after the quench, rather they slowly evolve towards it via coarsening dynamics [7, 10]. The discussion about this phase ordering kinetics will be addressed in section 1.4.

In the vicinity of the critical point related to a continuous transition, a system encounters various interesting phenomena, referred to as the critical phenomena [1–3, 5, 6, 9, 11–14]. Some non-trivial facts related to this phenomena are described in the next section.

1.2 Critical Phenomena: A Brief Outline

There are several anomalies in the thermodynamic properties of systems near the critical point [1, 2, 5]. Various measurable static and dynamic quantities show singular behaviour on approaching the critical neighbourhood. These are referred to as the *critical singu-*

larities [2, 5, 11–14]. These singularities are expressed mathematically as power-laws in terms of the reduced temperature, $\epsilon = \frac{T-T_c}{T_c}$, and external field H.

The power-law exponents, viz., $\alpha, \beta, \gamma, \delta, \eta, \nu$, of the static quantities [2, 11] are defined via the following equations.

$$\left.\begin{aligned} \text{Heat capacity} &: C \sim |\epsilon|^{-\alpha} && (1.1)\\ \text{Order parameter} &: M \sim \epsilon^{\beta} && (1.2)\\ \text{Susceptibility} &: \chi \sim |\epsilon|^{-\gamma} && (1.3)\\ \text{Correlation length} &: \xi \sim |\epsilon|^{-\nu} && (1.4) \end{aligned}\right\} \quad H = 0$$

$$\left.\text{Order parameter} : M \sim |H|^{1/\delta} \quad (1.5)\right\} \quad \epsilon = 0$$

The correlation function, $C(r)$, defined as [10]

$$C(r) = \langle \psi(\vec{r_1})\, \psi(\vec{r_2}) \rangle - \langle \psi(\vec{r_1}) \rangle \, \langle \psi(\vec{r_2}) \rangle, \tag{1.6}$$

follows the Ornstein-Zernike form

$$C(r) \sim r^{-p} \exp\left(-r/\xi\right), \tag{1.7}$$

where r is the scalar separation between the space points $\vec{r_1}$ and $\vec{r_2}$. In a d-dimensional space, the power-law exponent p is defined as [1, 2]

$$p = d - 2 + \eta. \tag{1.8}$$

The exponents ν and η refer to the behaviour of the $C(r)$ in the critical region. The critical exponent η is known as the *Fisher exponent* [1, 2]. The static quantity ξ [Eq. (2.20)] plays a crucial role in the critical phenomena, as it provides a measure of the length scale of fluctuations in the system.

The static critical exponents are connected to each other via various scaling laws [2, 3, 6]:

$$\text{Fisher equality} : \gamma = \nu(2 - \eta) \tag{1.9}$$

$$\text{Rushbrooke's identity} : \alpha + 2\beta + \gamma = 2 \tag{1.10}$$

$$\text{Widom's identity} : \gamma = \beta(\delta - 1) \tag{1.11}$$

$$\text{Josephson's identity} : \nu d = 2 - \alpha \tag{1.12}$$

These relations imply that all the exponents are not independent.

The critical exponents are independent of the material properties, or even the type of phase transition a system undergoes, and hence are universal in nature. This universality is captured by the *renormalization group* theory [3, 6], stating that near criticality the microscopic details of the systems become unimportant. However, the values of the exponents depend upon the spatial dimension, symmetry of the order parameter and the range of interactions. Depending on the type of interaction, there exists two *universality classes* [3, 6]. These universality classes and related exponents are as follows:

1. ***Short range or Ising Universality in space dimension*** $d = 3$***:***

   $$\alpha = 0.11, \quad \beta = 0.325, \quad \gamma = 1.239, \quad \nu = 0.63, \quad \delta = 5, \quad \eta = 0.035.$$

2. ***Long range or Classical Universality:***

   $$\alpha = 0, \quad \beta = \tfrac{1}{2}, \quad \gamma = 1, \quad \nu = \tfrac{1}{2}, \quad \delta = 3, \quad \eta = 0.$$

Understanding of the above mentioned static critical exponents are better than those for the dynamic counterpart. The primary quantity of interest in dynamic critical phenomena [5, 11] is the relaxation time τ. Near the critical point the systems witness diverging fluctuations and as a result the relaxation times of the systems diverge as

$$\tau \sim \xi^z. \tag{1.13}$$

This divergence in the relaxation time leads to critical slowing down. The value of the critical exponent z depends upon the type of ensemble or physical transition being studied [11, 15]. The dynamic exponents do not show universal behaviour as strong as the static exponents [11, 15]. For example, value of z for phase-separating binary mixture is different from that undergoing para-to-ferromagnetic transition. However, both these systems are part of the same static universality class.

1.3 Potts Model and Related Critical Phenomena

In this thesis, the discussion moves around the 2D q-state Potts model that has the Hamiltonian [16, 17]

$$\mathcal{H} = -J \sum_{\langle ij \rangle} \delta_{S_i, S_j}, \quad S_i = 1, 2, ..., q, \tag{1.14}$$

where J is the interaction strength, δ_{S_i,S_j} is the Kronecker delta and $\langle ij \rangle$ represents summation over nearest neighbour spins S_i. Here $J > 0$ corresponds to ferromagnetic interaction. The q-state Potts model has q number of possible states. This model is a generalization of the 2-dimensional Ising model, the Hamiltonian [7, 10] of which is given as

$$\mathcal{H}_{Ising} = -J \sum_{\langle ij \rangle} S_i S_j, \quad S_i = \pm 1, \tag{1.15}$$

where $+1$ and -1 are the only two possible values of S_i, representing up and down states of spins, respectively, at the lattice site i.

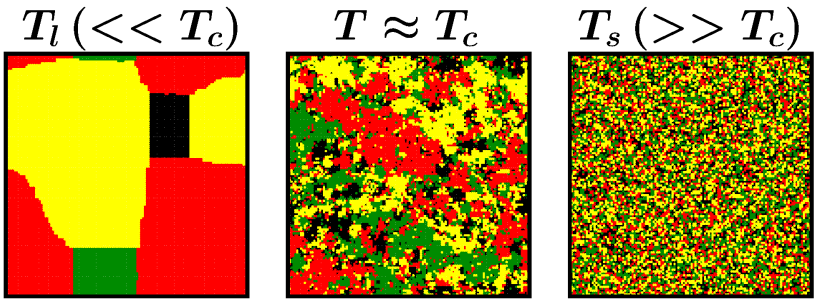

Figure 1.5: Generic configurations of 2D $q = 4$ state Potts ferromagnet, simulated on a square lattice having linear size $L = 128$ in each direction, at temperatures below, near and above T_c. The states of the spins at each of the L^2 lattice sites can have 4 possible values that are depicted here by different colours. These results were obtained via Glauber Monte Carlo simulations that will be defined later. The configuration for $T_l\,(<< T_c)$ represents a nonequilibrium situation.

Nevertheless, there exists some difference between the Ising model and the Potts model with $q = 2$. One way to realize this is the following. For $q = 2$, considering $S_i = \pm 1$, the Potts model Hamiltonian $\mathcal{H}$ can be rewritten as [18],

$$\mathcal{H} = -J \sum_{\langle ij \rangle} \frac{1}{2}(1 + S_i S_j) \tag{1.16}$$

$$= -\frac{J}{2} - \frac{J}{2} \sum_{<ij>} S_i S_j \tag{1.17}$$

$$= const + \frac{1}{2}\mathcal{H}_{Ising}. \tag{1.18}$$

Thus, the Hamiltonian of the Potts model for $q = 2$ provides essentially half the value of that of the Ising model. Unlike the Ising one, the exact solutions for $q \geq 3$ of the

Potts model is not known. However, many important features can be extracted, like the transition temperature T_c [19], which is given by

$$T_c = J/[k_B \ln(1+\sqrt{q})], \quad \text{for } q \geq 4, \tag{1.19}$$

k_B being the Boltzmann constant. Note that T_c can have a first or a second-order character depending upon the value of q.

The Potts model captures a variety of critical behaviours [19–22]. It undergoes second-order phase transition, exhibiting critical phenomena for $q \leq 4$ [16, 17, 19]. For $q = 2$, the model being equivalent to the Ising model, shares the same critical exponents, thus, belonging to the Ising universality class. For both $q = 3$ and 4, the critical exponents, however, are different from the above class [20, 21]. The model undergoes a first-order transition [16, 17, 19] for $q > 4$. For $q = 5$ and 6, the model exhibits weak first-order transitions, and thus show *pseudo-critical* phenomena [21]. For space dimension $d = 2$, some of the static critical exponents of $q = 2$, 3 and 4 are tabulated below [23].

q	α	β	γ	ν
2 (Ising)	0	$\frac{1}{8}$	$\frac{7}{4}$	1
3	$\frac{1}{3}$	$\frac{1}{9}$	$\frac{13}{9}$	$\frac{5}{6}$
4	$\frac{2}{3}$	$\frac{1}{12}$	$\frac{7}{6}$	$\frac{2}{3}$

Table 1.1: Critical exponents for the Ising model, as well as for the 3 and 4-state Potts model in two-dimensional space.

Several studies have been carried out on the critical dynamics of the q-state Potts model. The dynamic exponent z (≈ 2.16) for the 2-dimensional Potts model, exhibits a universal behaviour, as, it is, interestingly, independent of the value of the number of states q [21, 22].

1.4 Phase Ordering Kinetics

The dynamics of the evolution of a system from a thermodynamically unstable disordered state to a new equilibrium state is referred to as 'coarsening dynamics' or 'phase ordering dynamics' [7, 10]. During this evolution, ordered regions, called domains, rich in particles or spins of the same kind, are formed. The characteristic length scale, ℓ, i.e., the average size of the domains, grows with time. The structure or pattern formed by these domains is characterised by the two-point equal-time correlation function, $C(\vec{r},t)$. For isotropic systems $C(\vec{r},t) \equiv C(r,t)$ and it is defined as [10]

$$C(r,t) = \langle \psi(\vec{r},t)\ \psi(\vec{0},t)\rangle - \langle \psi(\vec{r},t)\rangle\ \langle \psi(\vec{0},t)\rangle, \tag{1.20}$$

where r $(= |\vec{r}|)$ is the separation between the two space points under consideration and $\psi(\vec{r},t)$, as stated before, is an appropriate order parameter which is both time and space dependent because of nonequilibrium nature of the system. In experiments, the correlation function cannot be directly measured. Instead, the Fourier transform of the correlation function, viz., the structure factor, $S(\vec{k},t)$, is measured, via probes like X-ray or neutron in small-angle scattering experiments. $S(\vec{k},t)$ is defined as [10]

$$S(\vec{k},t) = \int d\vec{r}\, e^{i\vec{k}.\vec{r}}\, C(\vec{r},t), \tag{1.21}$$

where $\vec{k}$ is the wave vector. In systems with isotropy, $S(\vec{k},t) \equiv S(k,t)$.

The correlation function and the structure factor usually exhibit the scaling property [7, 10]

$$C(r,t) \equiv \widetilde{C}(r/\ell(t)), \tag{1.22}$$

and

$$S(k,t) \equiv \ell^d(t)\ \widetilde{S}(k\ell(t)), \tag{1.23}$$

respectively, where $\widetilde{C}$ and $\widetilde{S}$ are time independent master functions. The characteristic length scale typically grows with time in a power-law fashion [7, 10]:

$$\ell(t) \sim t^{\alpha}. \tag{1.24}$$

The scaling properties in Eqs. (1.22) and (1.23) imply that the growth of domains in an ordering system follows a self-similar behaviour [10]. The domain structures at two instances are different from each other only by the change of a length scale. The value of the exponent α depends on several factors [10] like system dimentionality, order parameter symmetry, conservation of the order parameter and so on. The classification of the dynamics on the basis of conservation of order parameter during the coarsening of the system is discussed next.

1.4.1 Non-conserved Order-Parameter (NCOP) Dynamics

During NCOP dynamics, the total order parameter of the system, during ordering, is time dependent [7, 10]. A typical example of such dynamics is the phase ordering in a ferromagnet. We resort to this particular example for further discussions in this subsection.

The dynamics of an ordering ferromagnet can be modelled via the q-state Potts model [Eq. (1.14)], by implementing the spin-flip Glauber dynamics [24]. The evolution of the two-dimensional nearest neighbour $q = 4$ state Potts model, quenched from temperature $T_s = \infty$ to temperature $T_l = 0.5\,T_c$, obtained from Monte Carlo Simulations [15, 25] (details povided later) using Glauber spin-flip mechanism, is depicted in Fig. 1.6. The system is seen to evolve from a paramagnetic phase, where the spins are randomly arranged, towards ferromagnetic ordering after lowering the temperature.

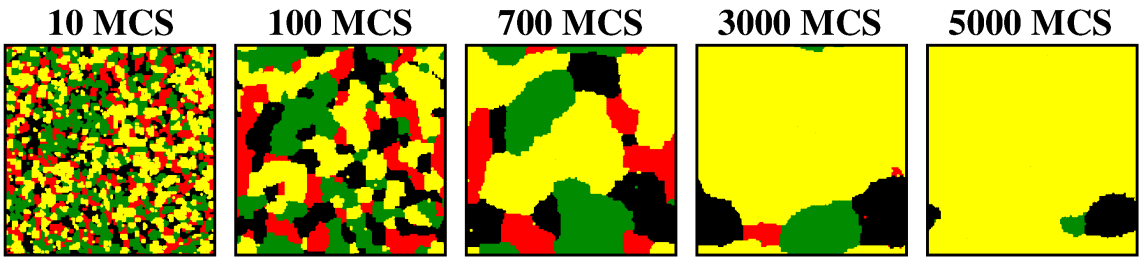

Figure 1.6: Snapshots from Monte Carlo simulations of the 2D $q = 4$ state Potts model, with Glauber dynamics. The four different coloured regions identify the four different states. Time is expressed in units of the Monte Carlo Steps (MCS). These snapshots are recorded during evolution of a system following a quench from $T_s = \infty$ to $T_l = 0.5\,T_c$.

The domain growth is due to the curvature driven motion of the interfaces, i.e., the domain boundaries. In order to reduce the free energy of the system, the interfaces move with a velocity, say, v. According to Allen-Cahn equation of motion of the interfaces

[7, 10, 26],

$$v = -K, \tag{1.25}$$

where K is the local curvature of the interface. For the average domain size of length $\ell(t)$, the above equation can be written as

$$\frac{d\ell(t)}{dt} \propto \frac{1}{\ell(t)}, \tag{1.26}$$

which gives [7, 10, 26, 27],

$$\ell(t) \sim t^{1/2}, \tag{1.27}$$

and is referred to as the Allen-Cahn law.

1.4.2 Conserved Order-Parameter (COP) Dynamics

The total order parameter of the system during the COP dynamics is independent of time [7, 10]. Here we will consider the example of phase separation in a multi-component mixture for further discussions.

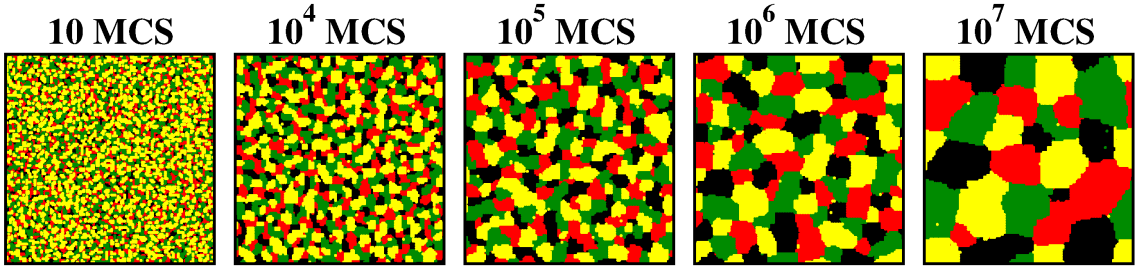

Figure 1.7: Snapshots from Kawasaki exchange Monte Carlo simulations of the two-dimensional $q = 4$ state Potts model. The different coloured regions show particles A, B, C, D, respectively. The quench protocol here is same as that in Fig. 1.6.

The dynamics of the phase separation process can be modelled using the q-state Potts model Hamiltonian [Eq. (1.14)], via the spin-exchange Kawasaki dynamics [28]. The states S_i in $\mathcal{H}$ [Eq. (1.14)] can now be considered to be equivalent to particles of different species, say, A, B, C and so on. In spin-exchange Kawasaki dynamics, two neighbouring particles are interchanged. The snapshots in Fig. 1.7 correspond to the two-dimensional nearest neighbour $q = 4$ state Potts model, quenched from temperature

$T_s = \infty$ to temperature $T_l = 0.5\,T_c$. These were obtained from Monte Carlo Simulations (details are provided later) using Kawasaki spin-exchange mechanism [15]. The evolution snapshots replicate the phase separation in quaternary mixtures. For this dynamics [29–33] average size of domains grow as $\ell(t) \sim t^{1/3}$.

1.5 Mpemba Effect: A Brief History

Mpemba Effect refers to a phenomenon where hot water freezes faster than cold water [34, 35]. The name of the effect is tributed to the then Tanzanian student, Erasto B. Mpemba, who, in early 1960s, observed that a cup of hot milk had turned into ice-cream faster than a cup of cold milk, on placing both of them in the refrigerator at the same time [34]. This old and counterintutive phenomena had known practical applications even at the time of Arisotle [36]. Mpemba and Osborne in the year 1969 showed that the time taken by water to start freezing decreases with an increase in the initial temperature of water. This effect is not only restricted to an ice-water system, but has recently been observed to exist in cooling granular gases [37], colloidal systems [38], spin glasses [39], etc. It is expected that this effect is associated with slowly evolving systems having glass-like complex energy landscape. Further details will be provided in chapter 2.

1.6 Motivation of the Work

Recently, over the period of a decade, scientists have been interested in generalizing the Mpemba effect [40]. In the phase transition community, there has been growing interest in finding the effect in transitions of different types. There exists a belief that frustration/metastability is essential for the appearance of the effect. However, very recently it was shown that this effect exists in simple Ising ferromagnet [41], having no in-built frustration! As an important extension of this even more counterintutive observation, we have been investigating the role of the existence of the "critical point" in deciding the presence or absence of the effect. For this purpose, the study of the Potts model, whose $q = 2$ corresponds to the Ising model, is important. The importance, in this context, lies in the fact that beyond $q = 4$ the transition loses its "critical" character. This is an interesting new direction of research that can offer appropriate understanding of this puzzling effect.

1.7 Overview of the Thesis

We examine the existence of Mpemba Effect in the 2-dimensional q-state ferromagnetic Potts model, for $q = 3, 5, 7$ and 10. We prepare systems at different starting temperatures T_s, which lie above T_c. The spin values of these systems are made to constitute of all states in nearly equal proportions. The prepared systems are then instantaneously quenched to a lower temperature T_l, inside the ordered region.

In **chapter 2**, we elaborate on the methodologies used.

In **chapter 3**, we first present the thermodynamic critical properties of the systems by preparing them at a set of different T_s. We then quench these systems to T_l and showcase the observations for each of the studied q values. At the end of this chapter we summarize the results of this thesis.

References

[1] M.E. Fisher, Rep. Prog. Phys. **30**, 615 (1967).

[2] H.E. Stanley, *Introduction to Phase Transitions and Critical Phenomena* (Clarendon Press, Oxford, 1971).

[3] N. Goldenfeld, *Lectures on Phase Transitions and the Renormalization Group* (West view press, 1992).

[4] J.M. Yeomans, *Statistical mechanics of phase transitions* (Clarendon, Oxford, 1992).

[5] A. Onuki, *Phase Transition Dynamics* (Cambridge University Press, Cambridge, 2002).

[6] M. Plischke and B. Bergersen, *Equilibrium Statistical Mechanics* (World Scientific, Singapore, 2006).

[7] *Kinetics of Phase transition*, edited by S. Puri and V. Wadhawan (CRC Press, Boca Raton, 2009).

[8] K. Binder, in *Phase Transformation of Materials*, edited by R.W. Cahn, P. Haasen and E.J. Kramer, vol. 5. p. 405 (Wiley VCH,Weinheim, 1991).

[9] L.P. Kadanoff, *Critical behavior, universality and scaling*, proceedings of the 1970 Varenna summer school on critical phenomena, edited by M.S. Green (Academic Press, New York, 1971).

[10] A.J. Bray, Adv. Phys. **51**, 481 (2002).

[11] P.C. Hohenberg and B.I. Halperin, Rev. Mod. Phys. **49**, 435 (1977).

[12] M.E. Fisher, in *Critical Phenomena*, edited by M.S. Green (Academic, London, 1971) p1.

[13] V. Privman, P.C. Hohenberg, and A. Aharony, in *Phase Transitions and Critical Phenomena*, edited by C. Domb and J.L. Lebowitz (Academic Press, New York, 1991), Vol. 14, Chap. I.

[14] C. Domb and D.L. Hunter, *On critical behavior of ferromagnets*, P. Phys. Soc. Lond. **86**, 1147 (1965).

[15] D.P. Landau and K. Binder, *A Guide to Monte Carlo Simulations in Statistical Physics* (Cambridge University Press, 2009).

[16] R.B. Potts, Proc. Camb. Phil Soc. **48**(1), 106 (1952).

[17] T. Kihara, Y. Midzuno, and T. Shizume, J. Phys. Soc. Japan **9**, 681 (1954).

[18] F. Chippari, *Dynamics for large q-Potts model in 2d*, Master's Degree thesis in Physics of Complex Systems, Politecnico Di Torino (2019-2020).

[19] F.Y. Wu, Rev. Mod. Phys. **54**, 235 (1982).

[20] S. Fan and F. Zhong, Phys. Rev. E **76**, 041141 (2007).

[21] K. Binder, J. Stat. Phys. **24**, pp. 69-86 (1981).

[22] O.F. de Alcantara Bonfim, EPL **4**, 373 (1987).

[23] B. Berche, P. Butera, W. Janke, and L. Shchur, arXiv:0809.5045 (2008).

[24] R.J. Glauber, J. Math. Phys. **4**, 294 (1963).

[25] K. Binder and D.W. Heermann, *Monte Carlo Simulation in Statistical Physics* (Springer, Berlin, 1997).

[26] S.M. Allen and J.W. Cahn, Acta Metall. **27**, 1085 (1979).

[27] G.S. Grest, M.P. Anderson, and D.J. Srolovitz, Phys. Rev. B **38**, 4752 (1988).

[28] K. Kawasaki, in *Phase Transition and Critical Phenomena*, edited by C. Domb and M.S. Green (Academic, New York, 1972), Vol. 2, p. 443.

[29] I.M. Lifshitz and V.V. Sloyozov, J. Phys. Chem. Solids. **19**, 35 (1961).

[30] C. Wagner, Z. Elektrochem. **65**, 581 (1961).

[31] S.K. Das and S. Puri, Phys. Rev. E **65**, 026141 (2002).

[32] W. Janke, S. Majumder, and S.K. Das, J. Phys.: Conf. Ser. **2122** 012009 (2021).

[33] S. Majumder, S.K. Das, and W. Janke, Phys. Rev. E **98**, 042142 (2018).

[34] E.B. Mpemba and D.G. Osborne, Phys. Educ. **4**, 172 (1969).

[35] M. Jeng, Am. J. Phys. **74**, 514 (2006).

[36] Aristotle, Meteorologica, ed. H. D. P. Lee, Harvard University Press, Book I, Chap. XII, pp. 85-87 (1962).

[37] A. Lasanta, F.V. Reyes, A. Prados, and A. Santos, Phy. Rev. Lett **119**, 148001 (2017).

[38] A. Kumar and J. Bechhoefer, Nature **584**, 64-68 (2020).

[39] M. Baity-Jesi, E. Calore, A. Cruz, L.A. Fernandez, J.M. Gil-Narvión, A. Gordillo-Guerrero, D. Iñiguez, A. Lasanta, A. Maiorano, E. Marinari, V. Martin-Mayor, J. Moreno-Gordo, A.M. Sudupe, D. Navarro, G. Parisi, S. Perez-Gaviro, F. Ricci Tersenghi, J.J. Ruiz-Lorenzo, S.F. Schifano, B. Seoane, A. Tarancoń, R. Tripiccione, and D. Yllanes, Proc. Natl. Acad. Sci. U. S. A. **116**, 15350 (2019).

[40] J. Bechhoefer, A. Kumar, and R. Chétrite, Nat. Rev. Phys. **3**, 534–535 (2021)

[41] N. Vadakkayil and S.K. Das, Phys. Chem. Chem. Phys. **23**, 19 (2021).

Chapter 2

Model, Methods, Observables and Analysis

2.1 Computational Details

In this thesis, Monte Carlo simulations [1–4] have been used extensively to study the kinetics of the q-state Potts model with Non-conserved Order-Parameter (NCOP) dynamics (see details in chapter 1, sec. 1.4.1). Below is a brief description of Monte Carlo simulations.

2.1.1 Monte Carlo Simulations

The thermal average of an observable A is defined, for N possible microstates, as [1, 2]

$$\langle A \rangle = \sum_{i=1}^{N} A_i P_i \tag{2.1}$$

where P_i is the probability of finding the system in the i^{th} state. In the canonical ensemble [1, 2]

$$P_i = \frac{e^{-\beta E_i}}{Z}, \tag{2.2}$$

where

$$Z = \sum_{i=1}^{N} e^{-\beta E_i} \tag{2.3}$$

is the partition function [1, 2], E_i is the energy of the i^{th} state and $\beta = 1/k_BT$, k_B being the Boltzmann constant. The exact calculation of $\langle A \rangle$ [Eq. (2.1)], using Eq. (2.2), can be analytically as well as computationally challenging, as it requires summing over all the possible microstates of the system. Monte Carlo technique devises an approximate method to calculate $\langle A \rangle$, escaping the challenges of finding Z.

In Monte Carlo simulations, instead of considering all the microstates, only a sequence of N' points are selected in the phase space according to the expected importance of the observations, $\{A_i\}$, at that point. This is called importance sampling [1, 2]. Each of these selected microstates are drawn from a probability distribution proportional to the Boltzmann factor, $e^{-\beta E_i}$. This idea reduces Eq. (2.1) to [1, 2]

$$\langle A \rangle = \frac{1}{N'} \sum_{i=1}^{N'} A_i. \tag{2.4}$$

In the limit $N' \to \infty$, ergodicity develops, and Eq. (2.4) resembles Eq. (2.1) with negligible statistical error.

In this exercise, the states are sampled according to the Markov Chain [1, 2], where the $(i+1)^{th}$ state is produced from the i^{th} state via a suitable transition probability $W_{i \to i+1}$, such that, in equilibrium

$$P_i \, W_{i \to i+1} = P_{i+1} \, W_{i+1 \to i}. \tag{2.5}$$

This is known as the detailed balance condition [1, 2]. The ratio of probabilities of transition from i^{th} to $(i+1)^{th}$ state and the corresponding return move is given by [1, 2]

$$\frac{W_{i \to i+1}}{W_{i+1 \to i}} = \frac{P_i}{P_{i+1}} = e^{-\beta(E_i - E_{i+1})} = e^{-\beta \Delta E}. \tag{2.6}$$

This ratio depends only on the energy difference ΔE $(= E_i - E_{i+1})$, between the two states.

The two most commonly used choices of W are [1, 2]

1. **Metropolis transition rate:** $W_{i \to i+1} = \begin{cases} e^{-\beta \Delta E}, & \text{if } \Delta E \geq 0 \\ 1, & \text{otherwise} \end{cases}$

2. **Glauber transition rate:** $W_{i \to i+1} = \frac{e^{\beta \Delta E}}{1 + e^{-\beta \Delta E}}$.

We will use Metropolis transition rate as the acceptance criteria for a move $i \rightarrow i+1$. The steps of the Metropolis algorithm are as follows, say, for Potts magnets in a lattice [1]:

1. An initial configuration is generated.

2. A random lattice site is chosen and the state of the spin located there is changed to any one of the other $q-1$ states, randomly. This is referred to as the trial move. This leads to NCOP dynamics. To establish Conserved Order-Parameter (COP) dynamics (details in chapter 1, sec. 1.4.2), two random neighbouring lattice sites are selected and their spins are interchanged.

3. The energies are calculated before and after each trial move using the Potts Hamiltonian [Eq. (1.14)].

4. For acceptance of the trial moves, the Boltzmann factor ($e^{-\beta\Delta E}$) is calculated and compared with a random number, say r, lying between 0 and 1. If $r \leq$ Boltzmann factor, the move is accepted.

5. Steps 2 to 4 are repeated L^2 times, L being the side of the square lattice. Trials of L^2 spins correspond to one Monte Carlo step (MCS).

In the vicinity of T_c, due to critical slowing down of the system, the use of standard Monte Carlo methods makes the computation time consuming. In order to overcome this difficulty cluster flipping methods can be used, if dynamics is not of concern. We resort to Wolff cluster flipping method [1, 5] to generate configurations near T_c in this dissertation.

2.1.2 Wolff Algorithm

1. An initial configuration is generated.

2. A random lattice site is chosen.

3. For the chosen site, all nearest neighbours with equal spin states are identified and added with a probability, $p = 1 - e^{-\beta J}$, to a cluster.

4. The above step is extended to the nearest neighbours of each lattice site that gets added in the cluster.

5. The spin state of all the lattice sites added in the cluster are changed to any one of the other $q-1$ available states. This completes one Wolff step.

Wolff algorithm is a rejection-free approach that helps in reducing the relaxation time of the system significantly, thus, making it very effective near T_c.

2.2 Protocol for Mpemba Effect

2.2.1 Mpemba Effect: The Counterintuitive Phenomena

Consider two systems prepared at starting temperatures T_{s_1} and T_{s_2}, respectively, such that $T_{s_1} > T_{s_2}$. According to the Mpemba effect [6–11], the time taken to equilibrate, following quenches to a common lower temperature T_l, is comparatively shorter for the system starting at T_{s_1} than the system at T_{s_2}. Despite the most intuitive expectation that a relatively colder object should cool faster than the hotter one, under the same applied conditions, there has been experiments that show the possibility of this unintuitive effect to exist [6–11]. Although this effect was rediscovered in the 1960s by Erasto Mpemba and Denis Osborne through their experiment on freezing of water [6], yet the first known mention of this effect dates back to 350 B.C., see book I, part 12 of *Meteorology* by Aristotle [12]. In his book the Greek philosopher mentioned that "to cool hot water quickly, begin by putting it in the sun". Reference of this effect also exists in the historical works of other philosophers like Roger Bacon [13], Sir Francis Bacon [14] and René Descartes [15].

Previously it was expected that this effect is limited to liquid systems, like, water or milk [6, 12, 13, 15–17]. There have been proposals to unveil the cause of this effect. For water, possible explanations have been tried on the basis of the concept of supercooling [18], evaporation [19], convection [20], hydrogen bond relaxation [21, 22] and so on, but a conclusion in this regard is still pending. In view of the reason that even factors like the presence of impurity in the substance can lead to large variation in observations of its freezing, it becomes difficult to reproduce experimental results [23]. This has led to debates. Infact, there also exist arguments against the very existence of this effect [24].

With the advancement of researches in this area, scientists have witnessed this effect to exist in systems of various kinds. There are experimental reports that assert this effect to exist in systems with phase transitions like polymers [25], magnetic alloys [26], clathrate hydrates [27], and also in systems like colloids [28] without any phase transition. Mpemba-like behaviour has also been observed in numerical simulations [28] of granular

gases [29–31], carbon nanotube resonators [32], cold gases [33], spin glasses [34], quantum systems [35] and Ising ferromagnets [36]. In the cases of Mpemba-like observation in frustrated systems like spin glasses, as well as, in simple systems with no in-built frustrations like Ising ferromagnet, change in correlation length (ξ) exists in the systems with different starting temperatures T_s [34, 36–38]. It is perceived that certain anomalies must be present in the systems to observe Mpemba effect [34, 36]. The observation of Mpemba effect in Ising model, with which a large variety of condensed-matter systems, like binary mixtures and liquid-gas transitions, can be studied, provides a promising new direction for research on this effect [23].

2.2.2 Models and Method

We will inspect whether Mpemba Effect exists in our model of interest: the q-state Potts model in 2-dimensional space. The Hamiltonian $\mathcal{H}$ and transition temperature T_c [39] of this model, as stated in chapter 1, are given by

$$\mathcal{H} = -J \sum_{\langle ij \rangle} \delta_{S_i,S_j}, \quad S_i = 1, 2, ..., q, \tag{2.7}$$

and

$$T_c = J/[k_B \ln(1 + \sqrt{q})], \tag{2.8}$$

respectively. Here J is the interaction strength, $\langle ij \rangle$ represents summation over nearest neighbours, δ_{S_i,S_j} is the Kronecker delta and k_B is the Boltzmann constant.

The protocol followed to investigate the presence of Mpemba Effect in this model comprises of two parts:

1. System preparation at different starting temperatures T_s.

2. Quenching the systems to a common lower temperature T_l.

We choose a set of temperatures above T_c for preparing the systems. Some of these are quite close to T_c. The spatial fluctuations and hence ξ diverges at $T = T_c$ [36, 40, 41]. It will, thus, be appropriate to inspect whether the variation of structure related parameters are crucial to account for the observation of this effect. As stated above, in order to prepare the systems at temperatures near T_c, we use Wolff algorithm (subsec. 2.1.2), where a cluster of equal spins is flipped at one go. This algorithm helps avoiding strong

critical slowing down of the system. These prepared systems are made to have critical concentration with all states in nearly equal proportions. We then instantaneously quench the prepared systems to T_l. The approach to the equilibrium at T_l is simulated via the Monte Carlo Simulations (subsec. 2.1.1) with the Glauber spin-flip mechanism. The energy decay and the growth of the systems, as they slowly relax to the new equilibrium state, are recorded in order to investigate Mpemba effect.

We perform this exercise for $q = 3, 5, 7$ and 10. Some basic results are presented for $q = 2$ as well. Periodic boundary conditions are applied in all directions of the systems.

2.3 Observables and Estimations

We will investigate some of the thermodynamic properties, like magnetization per spin (M), susceptibility (χ), structure factor ($S(k)$) and correlation length (ξ), of the initially prepared systems in the results chapter. The morphology of a system is characterized by the two-point equal time correlation function, $C(\vec{r}, t)$. For an isotropic system with order parameter $m(\vec{r}, t)$, the two-point correlation function, $C(r, t)$, as a function of the separation (r) between the two space points is calculated as [42]

$$C(r,t) = \langle m(\vec{r},t)\, m(\vec{0},t)\rangle - \langle m\rangle^2\,; \quad r = |\vec{r}|. \tag{2.9}$$

The order parameter or magnetization for q-state Potts model can be defined as [43, 44]

$$m = \frac{\sum_{i=1}^{N} [\, q\, \delta_{S_i,1} - 1]}{N(q-1)}, \tag{2.10}$$

where N is the number of spins in the lattice. Here $\delta_{S_i,1}$ represents the following:

$$\delta_{S_i,1} = \begin{cases} 1, & \text{if spin at site } i, \text{ i.e., } S_i = 1 \\ 0, & \text{otherwise.} \end{cases}$$

Note that 1 is just a representative number. Eq. (2.10) can be rewritten as

$$m = \frac{q\left[\sum_{i=1}^{N} \delta_{S_i,1} - \frac{N}{q}\right]}{N(q-1)} \tag{2.11}$$

$$= \frac{q}{q-1}\left[\langle \delta_{S_i,1}\rangle - \frac{1}{q}\right]. \tag{2.12}$$

Below T_c, when a system is ordered and all spins assume value corresponding to one particular state, then $\langle \delta_{S_i,1} \rangle = 0$ or 1. The minimum and maximum possible values of magnetization [Eq. (2.12)] are

$$m_{\min} = \frac{q}{q-1}\left[0 - \frac{1}{q}\right] = \frac{-1}{q-1}, \tag{2.13}$$

and

$$m_{\max} = \frac{q}{q-1}\left[1 - \frac{1}{q}\right] = 1, \tag{2.14}$$

respectively. Above T_c, the system is homogeneous and the possibility of finding $S_i = 1$, at any site i is $1/q$, i.e., $\langle \delta_{Si,1} \rangle = 1/q$. Therefore, Eq. (2.12) reduces to $m = 0$ at temperatures above T_c. The magnetisation distribution of the systems for temperatures below T_c will essentially have two peaks corresponding to $m_{\min}$ and $m_{\max}$. These peaks will continue to shift towards each other with increase in temperature, and for $T > T_c$, in the disordered regime, they merge to form a single peak. However, $m_{\max}$ is obtained only when $S_i = 1$ (according to the used definition in Eq. (2.10)). This makes the height of the peak corresponding to $m_{\max}$ to be shorter than the height of the peak corresponding to $m_{\min}$.

The fluctuations in the order parameter at $T > T_c$, once equilibrium is attained, gives a measure of susceptibility χ, defined as [43]

$$k_B\, T\, \chi = \left(\frac{q-1}{q}\right)^2 [N\,(\langle m^2 \rangle - \langle m^2 \rangle)]. \tag{2.15}$$

For the q-state Potts model, $C(r,t)$ is defined as [45]

$$C(r,t) = \frac{q}{q-1}\left[\langle \delta_{S_i,S_j} \rangle - \frac{1}{q}\right]; \quad r = |i-j|. \tag{2.16}$$

This definition is appropriate in mimicking the morphology of the system. In the limit $r \to 0$, the value of $\langle \delta_{S_i,S_j} \rangle = 1$, thus resulting in $C(r,t) = 1$. In the limit $r \to \infty$, the possibility of finding the same spin at a distance r becomes less, providing $\langle \delta_{S_i,S_j} \rangle = 1/q$. Therefore, in large r limit, $C(r,t) = 0$.

The fourier transform of the correlation function is the structure factor [42]

$$S(\vec{k},t) = \int d\vec{r}\, e^{i\vec{k}.\vec{r}}\, C(\vec{r},t), \tag{2.17}$$

and can be measured directly in scattering experiments, where $\vec{k}$ is the wave vector of the scattered light beam. The intensity of the scattered beam is proportional to the structure factor [46], that gets enhanced near the critical point. For isotropic systems $S(\vec{k},t) \equiv S(k,t)$. Close to the critical point, when all the states of the system are present in equal proportions, the structure factor (S(k)) gives a measure of spatial fluctuations in the concentration [47]. For temperatures very close to T_c, as $k \to 0$, $S(k)$ diverges. In the presence of correlated spatial fluctuations in the system with $\xi \sim \lambda_{light}$, say, the latter being the wavelength of the incident light, the beam gets totally scattered [46]. This results in an opaque appearance of the system and is known as critical opalescence. This phenomena is captured by the Ornstein-Zernike theory [41, 46], which describes $S(k)$ at small k limit as

$$S(k) = \frac{k_B\, T\, \chi}{1 + k^2\, \xi^2}. \tag{2.18}$$

As mentioned in chapter 1, in the thermodynamic limit, the critical behaviour of χ and ξ are defined as

$$\chi \sim |\epsilon|^{-\gamma} \tag{2.19}$$

and

$$\xi \sim |\epsilon|^{-\nu}, \tag{2.20}$$

respectively, where $\epsilon = \frac{T - T_c}{T_c}$ is the reduced temperature.

References

[1] D.P. Landau and K. Binder, *A Guide to Monte Carlo Simulations in Statistical Physics* (Cambridge University Press, 2009).

[2] K. Binder and D.W. Heermann, *Monte Carlo Simulation in Statistical Physics* (Springer, Berlin, 1997).

[3] M.E. Newman and G.T. Barkema, *Monte Carlo Methods in Statistical Physics* (Clarendon Press, Oxford, 1999).

[4] M.A. Novotny, Computers in Physics **9**, 46 (1995).

[5] U. Wolff, Phys. Rev. Lett. **62**, 361 (1989).

[6] E.B. Mpemba and D.G. Osborne, Phys. Educ. **4**, 172–175 (1969).

[7] I. Firth, Phys. Educ. **6**, 32–41 (1971).

[8] E. Deeson, Phys. Educ. **6**, 42–44 (1971).

[9] B. Wojciechowski, I. Owczarek, and G. Bednarz, Cryst. Res. Technol. **23**, 843–848 (1988).

[10] J. Walker, Sci. Am. **237**, 246–257 (1977).

[11] D. Auerbach, Am. J. Phys. **63**, 882–885 (1995).

[12] Aristotle, *Meteorologica*, translated by H.D.P. Lee Harvard U.P., London, Book I, Chap. XII, pp. 85–87 (1962).

[13] R. Bacon, *The Opus Majus of Roger Bacon*, translated by Robert Belle Burke (Russell and Russell, New York, 1962), Vol. II, Part 6, p. 584.

[14] F. Bacon, *The Physical and Metaphysical Works of Lord Francis Bacon*, edited by J. Devey (Bell, London, 1911), Book II, Chap. L, p. 559.

[15] R. Descartes, *Discourse on Method, Optics, Geometry, and Meteorology*, translated by P.J. Olscamp (Bobb-Merrill, Indianapolis, 1965), Chap. 1, p. 268.

[16] P. Zalden, F. Quirin, M. Schumacher, J. Siegel, S. Wei, A. Koc, M. Nicoul, M. Trigo, P. Andreasson, H. Enquist, M.J. Shu, T. Pardini, M. Chollet, D. Zhu, H. Lemke, I. Ronneberger, J. Larsson, A. M. Lindenberg, H. E. Fischer, S. Hau-Riege, D. A. Reis, R. Mazzarello, M. Wuttig and K. Sokolowski-Tinten, Science, **364**, 1062–1067 (2019).

[17] X.L. Phuah, W. Rheinheimer, Akriti, L. Dou and H. Wang, Scr. Mater., **195**, 113719 (2021).

[18] D. Auerbach, Am. J. Phys. **63**, 882 (1995).

[19] S.M. Mirabedin and F. Farhadi, Int. J. Refrig. **73**, 219 (2017).

[20] M. Vynnycky and S. Kimura, Int. J. Heat Mass Transf. **80**, 243 (2015).

[21] X. Zhang, Y. Huang, Z. Ma, Y. Zhou, J. Zhou, W. Zheng, Q. Jiang, and C. Q. Sun, Phys. Chem. Chem. Phys. **16**, 22995 (2014).

[22] Y. Tao, W. Zou, J. Jia, W. Li, and D. Cremer, J. Chem. Theory Comput. **13**, 55 (2017).

[23] J. Bechhoefer, A. Kumar, R. Chétrite, Nat Rev Phys. **3**, 534–535 (2021).

[24] H.C. Burridge and P.F. Linden, Sci. Rep. **6**, 37665 (2016).

[25] C. Hu, J. Li, S. Huang, H. Li, C. Luo, J. Chen, S. Jiang, and L. An, Cryst. Growth Des. **18**, 5757 (2018).

[26] P. Chaddah, S. Dash, K. Kumar, and A. Banerjee, arXiv preprint arXiv:1011.3598 (2010).

[27] Y.-H. Ahn, H. Kang, D.-Y. Koh, and H. Lee, Korean Journal of Chem. Eng. **33**, 1903-1907 (2016).

[28] A. Kumar and J. Bechhoefer, Nature **584**, 64–68 (2020).

[29] A. Lasanta, F.V. Reyes, A. Prados, and A. Santos, Phys. Rev. Lett. **119**, 148001 (2017).

[30] A. Torrente, M.A. López-Castaño, A. Lasanta, F.V. Reyes, A. Prados, and A. Santos, Phys.Rev. E **99**, 060901 (2019).

[31] A. Biswas, V.V. Prasad, O. Raz, and R. Rajesh Phys. Rev. E **102**, 012906.

[32] P. Greaney, G. Lani, G. Cicero, and J. Grossman, Metall. Mater. Trans. A **42**, 3907–3912 (2011).

[33] T. Keller, V. Torggler, S.B. Jäger, S. Schütz, H. Ritsch, and G. Morigi, New J. Phys. **20**, 025004 (2018).

[34] M. Baity-Jesi, E. Calore, A. Cruz, L.A. Fernandez, J.M. Gil-Narvión, A. Gordillo-Guerrero, D. Iñiguez, A. Lasanta, A. Maiorano, E. Marinari, V. Martin-Mayor, J. Moreno-Gordo, A.M. Sudupe, D. Navarro, G. Parisi, S. Perez-Gaviro, F. Ricci Tersenghi, J.J. Ruiz-Lorenzo, S.F. Schifano, B. Seoane, A. Tarancoń, R. Tripiccione, and D. Yllanes, Proc. Natl. Acad. Sci. U. S. A. **116**, 15350 (2019).

[35] A. Nava, and M. Fabrizio, Phys. Rev. B, **100**, 125102 (2019).

[36] N. Vadakkayil and S.K. Das, Phys. Chem. Chem. Phys. **23**, 19 (2021).

[37] K. Binder and A.P. Young, Rev. Mod. Phys. **58**, 801–976 (1986).

[38] H. Rieger, Annu. Rev. Comput. Phys. **2**, 295-341 (1925).

[39] F.Y. Wu, Rev. Mod. Phys. **54**, 235 (1982).

[40] A. Onuki, *Phase Transition Dynamics* (Cambridge University Press, Cambridge, UK, 2002).

[41] M.E. Fisher, Rep. Prog. Phys. **30**, 615 (1967).

[42] A.J. Bray, Adv. Phys. **51**, 481 (2002).

[43] K. Binder, J. Stat. Phys. **24**, pp. 69-86 (1981).

[44] A. Boer, Phys. A: Stat. Mech. Appl. **390**, 4203-4209 (2011)

[45] M.P.O. Loureiro, J.J. Arenzon, L.F. Cugliandolo, and A. Sicilia, Phys. Rev. E **81**, 021129 (2010).

[46] H.E. Stanley, *Introduction to Phase Transitions and Critical Phenomena* (Clarendon Press, Oxford, 1971).

[47] S.K. Das, J. Horbach, K. Binder, M.E. Fisher, and J.V. Sengers, J. Chem. Phys. **125**, 024506 (2006).

Chapter 3

Mpemba Effect in q-state Potts Magnets

3.1 A Brief Recapitulation and Overview

In order to provide a complete context for the discussions in this chapter, we briefly review some of the concepts already discussed in the previous chapters.

The work of Mpemba and Osborne [1] in 1969, showing faster freezing of hotter water, than a colder one, inspired similar investigations in other systems. In this drive, the 'generalized' Mpemba effect was identified in granular gases [2–4], spin glasses [5] and colloidal systems [6]. From some of these studies it seems that frustration or metastability is believed to be necessary for the observation of this puzzling phenomenon. Interestingly, in a recent work [7], Mpemba effect was shown to be present in a simple model system, viz., the Ising ferromagnet with a second-order phase transition. This system has no in-built frustration which indicates that the effect is rather common.

In this chapter, we are interested in investigating the presence of this effect in q-state Potts model that exhibits para-to ferromagnetic transitions of both kinds - first and second-order [8–14]. We consider two-dimensional ($d = 2$) systems prepared at a set of different starting temperatures, T_s, above the 'critical' temperature T_c and quench them to $T_l = 0.5\ T_c$, for $q = 3, 5, 7$ and 10. In $d = 2$, beyond $q = 4$ the phase transition in the model changes from second to first-order [8–14]. For both the varieties we look at the relaxation of the systems as they slowly approach the new equilibrium. The evolutions of the systems take place via the formation and growth of domains. The domain structures at two different instances are self-similar, at late enough times, and differ from each other only by the change of a characteristic length scale, $\ell(t)$. This self-similar behaviour is

captured by the scaling property of $C(r,t)$ [15, 16], viz.,

$$C(r,t) \equiv \widetilde{C}(r/\ell(t)), \tag{3.1}$$

the symbols having meanings similar to the ones mentioned earlier.

3.2 Model and Simulations

For the q-state Potts model, Table 3.1 gives [11] the approximate values of T_c in the thermodynamic limit, in units of J/k_B, for the studied values of q. Here J is the interaction strength and k_B is the Boltzmann constant. The Hamiltonian $\mathcal{H}$ and the mathematical expression for T_c of the model has been mentioned in Eq. (1.14) and Eq. (1.19), respectively.

q	T_c (J/k_B)
2	1.1346
3	0.9950
5	0.8515
7	0.7731
10	0.7012

Table 3.1: The values of the critical temperature, T_c, for the q-state Potts model, in two-dimensional space, have been listed for $q = 2, 3, 5, 7$ and 10.

As already mentioned, the initial configurations of Potts magnets are prepared at different starting temperatures T_s above T_c using the Wolff Cluster Algorithm. Corresponding morphology is characterised by the structure factor, $S(k,t)$. We calculate the latter via the fast Fourier transform (FFT) algorithm, using the relation [17]

$$S(k,t) = \langle\, \psi_k\,(t)\; \psi_{-k}(t)\,\rangle, \tag{3.2}$$

where $\psi_k(t)$ is the Fourier transform of the order parameter $\psi(\vec{r},t)$ $(= e^{i\,\theta(\vec{r})};\ \theta = \frac{2\pi n}{q},\ n = 1,\ldots,q)$.

The evolution of the two-dimensional q-state Potts model, following quench from a starting temperature T_s, to a lower temperature T_l, is studied via Monte Carlo simulations using Glauber spin-flip mechanism. The trial move of changing a randomly chosen spin to any of the other $q-1$ states is accepted by the standard Metropolis criterion [18]. For acceptance of the trial moves the Boltzmann factor is calculated and compared with a random number, say r, lying between 0 and 1. If $r \leq$ Boltzmann factor, the move is accepted. For $T_l = 0$, from which we present a limited set of results, if the energy after trial is less than or equal to the energy before, the move is accepted.

The system size is taken to be $L = 256$, L being the side of the square lattice. Thus, the total number of spins is given by L^2. Time is measured in units of Monte Carlo Steps (MCS). One MCS corresponds to the trials of L^2 spins.

The average domain length, $\ell(t)$, during the ferromagnetic evolution is calculated from the first moment of the domain size distribution function, $P(\ell_d)$ [19–21], i.e.,

$$\ell(t) = \int P(\ell_d, t)\ \ell_d\ d\,\ell_d, \tag{3.3}$$

where ℓ_d is the distance between two consecutive interfaces along the Cartesian directions. The morphology related calculations is done after the removal of thermal noise from the system. The procedure of noise elimination follows a majority spin rule [19, 20]. According to this rule, the spin value on a lattice site i is replaced by the spin value that is present in the majority amongst i and nearest neighbours of i.

All the data are averaged over runs with 18000 independent initial configurations. Periodic boundary conditions are applied along all possible directions of the system.

3.3 Calculation of Critical Properties

In the ordered region below T_c, the probability distribution, $P(m)$, of the order parameter, i.e., magnetisation, m, has a double-peak structure. We denote these peaks by $m_{\rm min}$ and $m_{\rm max}$. In Fig. 3.1, we show $P(m)$ versus m plots for the cases $q = 3$ and $q = 5$. The difference between the heights of the peaks is expected because of the bias in the definition of the order parameter. Furthermore, at a low temperature this gets affected by a strong barrier due to the interfacial free energy.

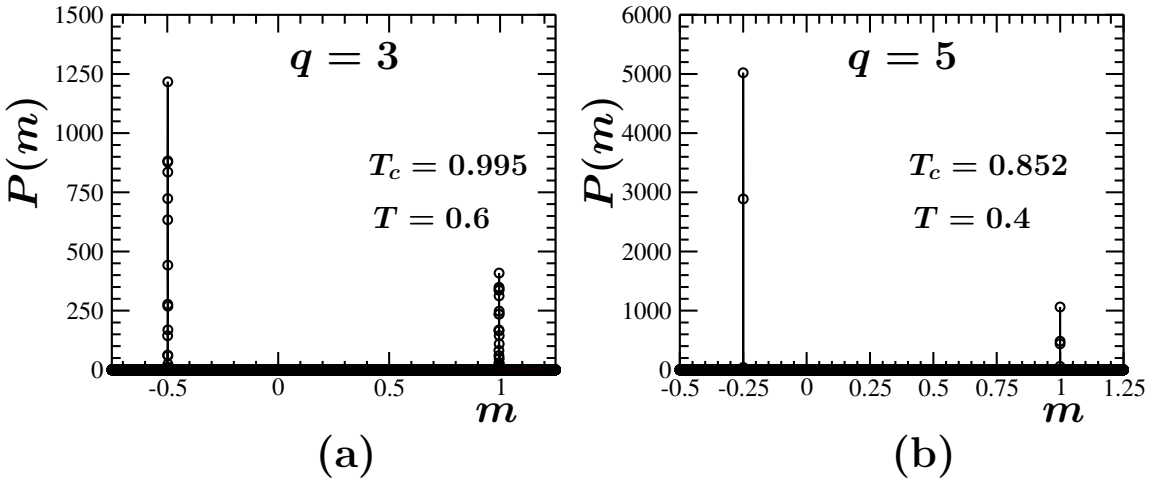

Figure 3.1: Probability distributions, $P(m)$, of the magnetisation m, for (a) $T = 0.6$, $q = 3$ and (b) $T = 0.4$, $q = 5$. The values of T_c in the thermodynamic limit for both these q values have been mentioned inside the respective frames.

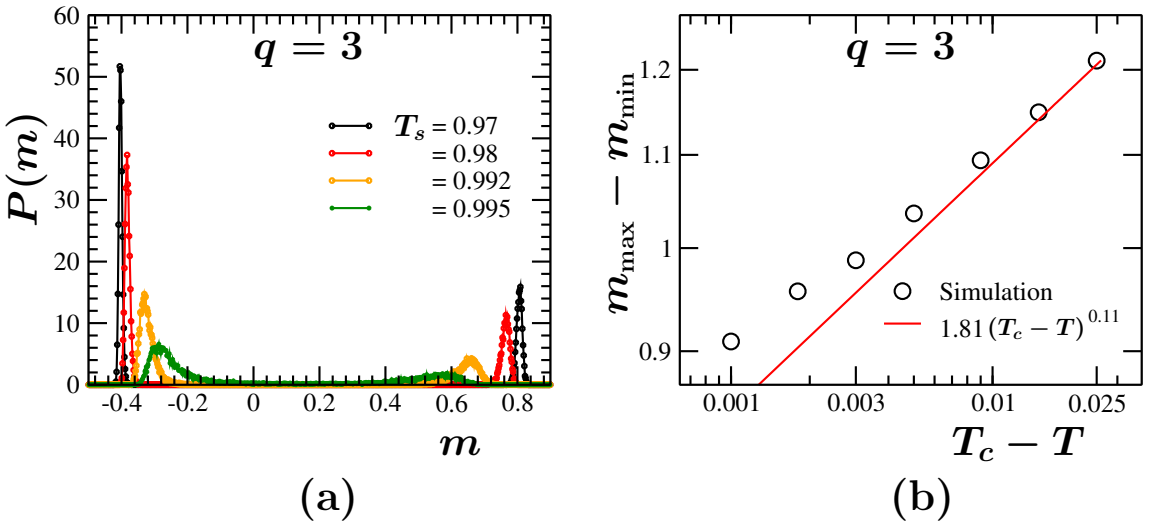

Figure 3.2: (a) Probability distributions, $P(m)$, of the magnetisation m for a set of temperatures below T_c, for $q = 3$. (b) Plot of $m_{\max} - m_{\min}$ versus $(T_c - T)$ for $q = 3$. The solid line represents Eq. (3.4), with $\beta = 0.11$, whereas the circles are the simulation results. These data are presented on a log-log scale. The discrepancies close to T_c are due to finite-size effects.

With the rise in temperature, these peaks shift towards each other as shown in Fig. 3.2a, for $q = 3$. Taking the temperature dependent locations of the peaks as points along the coexistence curves, we have constructed the corresponding phase diagram. In

Fig. 3.2b, we plot $m_{\max} - m_{\min}$ versus $(T_c - T)$. This is expected to vary as [22]

$$A\left(1 - \frac{T}{T_c}\right)^{\beta}, \tag{3.4}$$

where A is a critical amplitude and β is a critical exponent. Agreement of the simulation data with this form, for $\beta = 1/9$, the theoretically expected value [9, 10, 12, 14], is good. Deviations closer to T_c are due to finite-size effects [23].

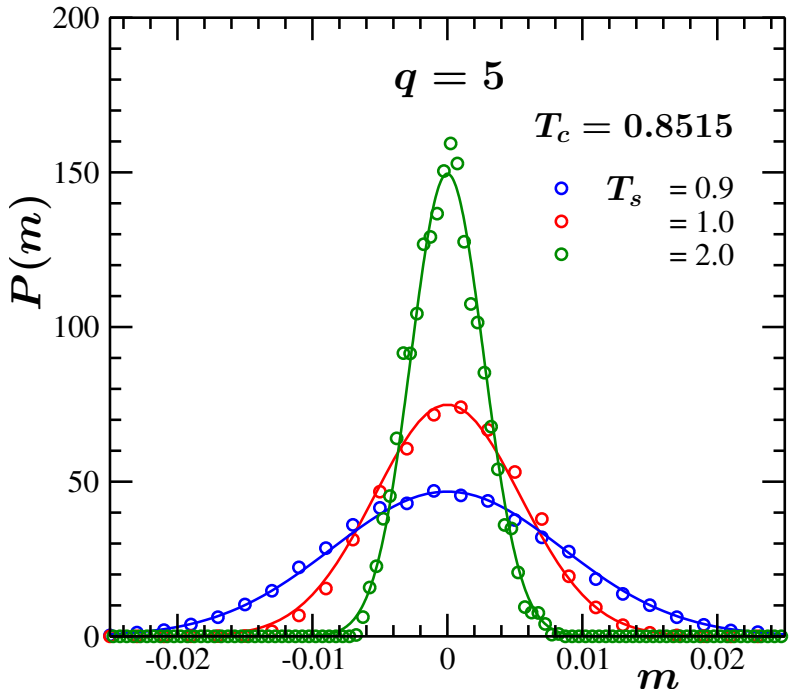

Figure 3.3: Probability distributions, $P(m)$, of magnetisation m, at three different temperatures T_s. The width of fluctuations is higher for temperatures closer to T_c. The solid lines represent Gaussian fits. These results are for $q = 5$.

At temperatures above T_c, the systems reside in the paramagnetic region of the phase diagram with the mean value of the magnetisation being zero. We choose a set of temperatures, T_s, in this region to prepare systems for the final quenches. In Fig. 3.3 we show the probability distributions concerning the fluctuations in the order parameter, m, using three such values of T_s for $q = 5$. The fluctuations in the order parameter can be noted from the widths of the Gaussian looking curves. This is strong very close to T_c and keeps on decreasing with increasing temperatures. From these fluctuations one can

measure the susceptibility χ. In the critical regime, χ diverges as the power law [22]

$$k_B T\chi = \Gamma \left|1 - \frac{T_c}{T}\right|^{-\gamma}, \tag{3.5}$$

where Γ is another critical amplitude and γ the critical exponent. Note that the value of the exponent remains same on approaching T_c from either side, i.e., T_c^+ or T_c^- [22]. However, the values of Γ differ in the two cases [22, 24]. On approaching T_c from T_c^+ for $q = 3$, it is expected that $\gamma = 13/9$ [9, 10, 12]. In Fig. 3.4, for temperatures T_s above T_c, we plot $k_B T_s \chi$ as a function of $\epsilon \left(= 1 - \frac{T_c}{T_s}\right)$. For $q = 2$ and 3, the phase transition being of second-order, χ diverges near T_c. Apparently, the enhancement gets weaker with increasing q. This is because the model loses its critical character beyond $q = 4$. Note that the solid lines in Fig. 3.4 have been plotted using Eq. (3.5), where Γ and γ, the adjustable parameters, for $q \geq 5$, are merely numbers which provide the best fits within the temperature regime.

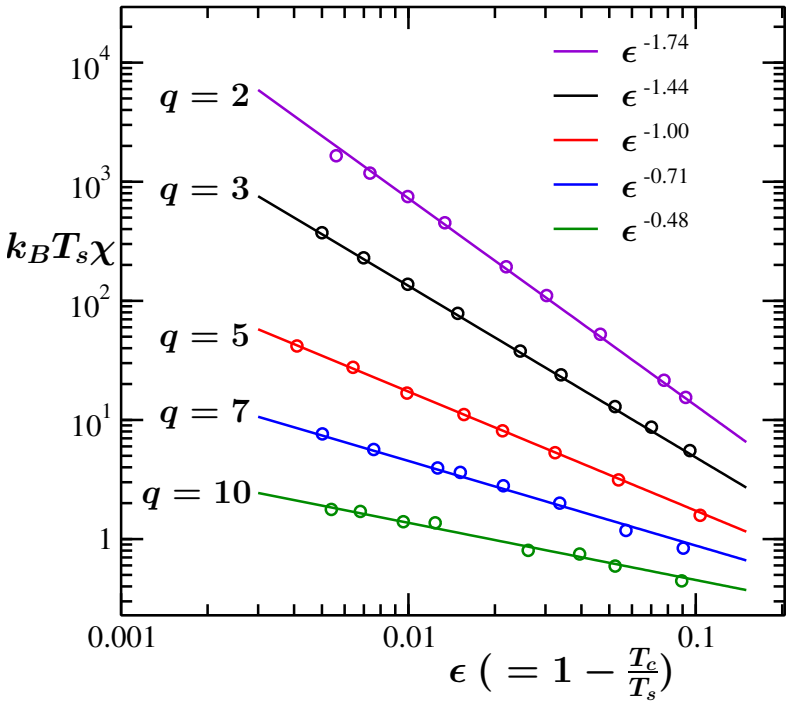

Figure 3.4: Susceptibility χ, multiplied by $k_B\, T_s$, is plotted versus the reduced temperature ϵ. Results for several values of q are included. The solid lines are power-laws with different values of γ and Γ.

Fig. 3.5a and 3.5b show equilibriated configurations of 3 and 5-state Potts models, respectively, obtained at T_s values as mentioned at the top of the frames. In both the

cases, the configurations have critical concentrations, i.e., all components are present in practically equal proportions. The variation of spatial correlations at different T_s can be recognized from the snapshots. It can be seen that with the increase in the value of T_s, i.e., on moving farther away from T_c, the spatial correlations in the system diminishes.

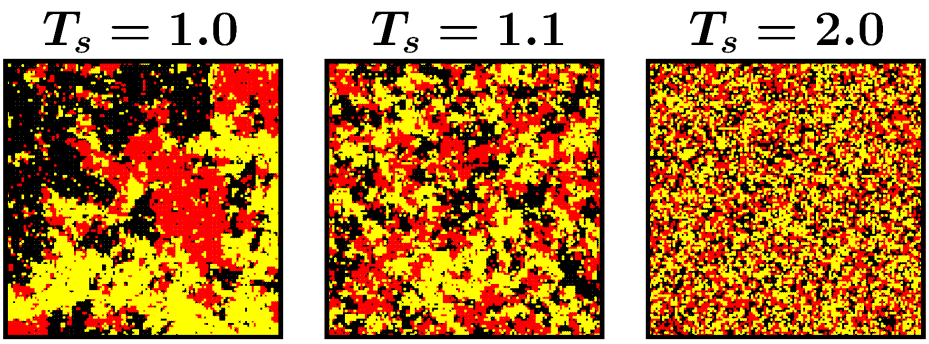

(a) 3-state Potts model.

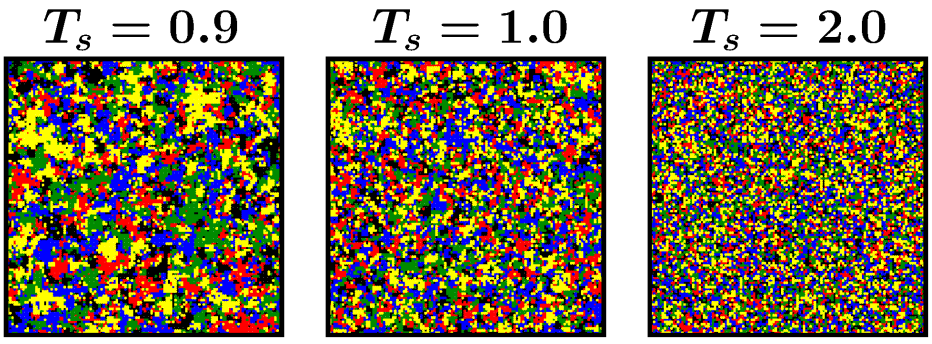

(b) 5-state Potts model.

Figure 3.5: Equilibrium snapshots of the q-state Potts model, for (a) $q = 3$ and (b) $q = 5$, at critical compositions. Different colours represent different states. In each of the cases, pictures from different T_s ($> Tc$) values have been included.

The presence of correlated spatial fluctuations in the system and its variation with temperature can be quantified via the calculation of structure factor. We have presented the plots of $S(k, t)$, as a function of k, in Fig. 3.6. The enhancement of $S(k, t)$ at small k with the approach of T_s to T_c, implies that the fluctuation is getting critical. In this regime $S(k, t)$ is described well by the Ornstein-Zernike relation [22, 25, 26],

$$S(k) = \frac{k_B\, T\, \chi}{1 + k^2\, \xi^2}, \tag{3.6}$$

where ξ is the correlation length.

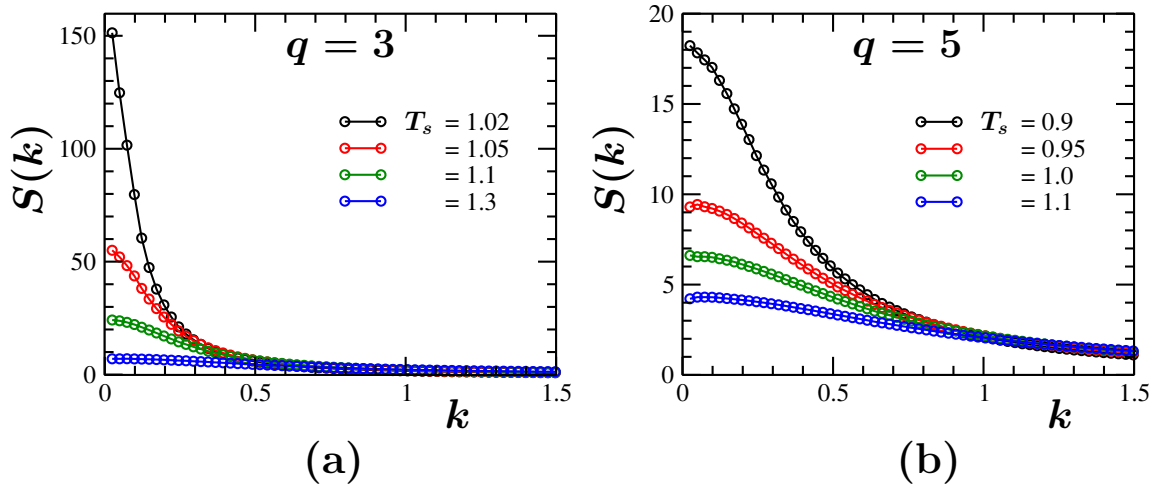

Figure 3.6: Plots of structure factor, $S(k)$, versus the wave number k, at critical compositions, for (a) $q = 3$ and (b) $q = 5$. Results from different T_s have been shown.

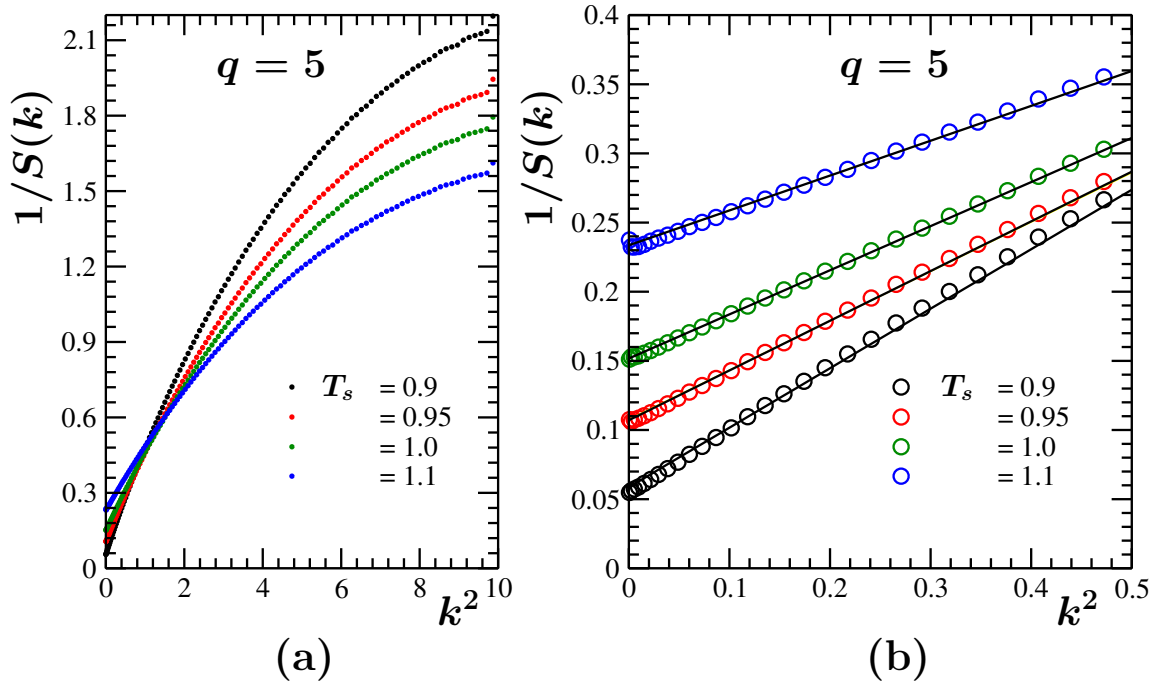

Figure 3.7: (a) Plots of $1/S(k)$ versus k^2, at various T_s, with critical concentrations, for the 5-state Potts model. In part (b) we provide an enlarged view of part (a), showing the linear behaviour of $1/S(k)$ at small k limit.

In Fig. 3.7a, we plot $1/S(k)$ as a function of k^2, for the 5-state Potts model. Fig. 3.7b is an enlarged version of Fig. 3.7a showing data only for very small k. The linear behaviour

in the $k \to 0$ region is in agreement with Eq. (3.6). The enhancement of susceptibility in the critical regime can be identified from the smaller values of the intercept of the $1/S(k)$ axis in Fig. 3.7b, with the decrease in temperature. The correlation length, ξ, of the system can be measured from the slope of these linear regions. The slope and hence ξ is seen to decease with the increase in temperature. As mentioned in chapter 2, ξ, at criticality, diverges as

$$\xi \sim |\epsilon|^{-\nu}, \tag{3.7}$$

where $\epsilon = \frac{T-T_c}{T_c}$ is the reduced temperature. This can be seen from Fig. 3.8. The divergence is rounded as the critical behaviour of the system is lost. The exponent ν for $q = 2$ and 3 are known to have values [14] 1 and 5/6. For other q values the shown exponents and amplitudes are merely the numbers in accordance with Eq. (3.7).

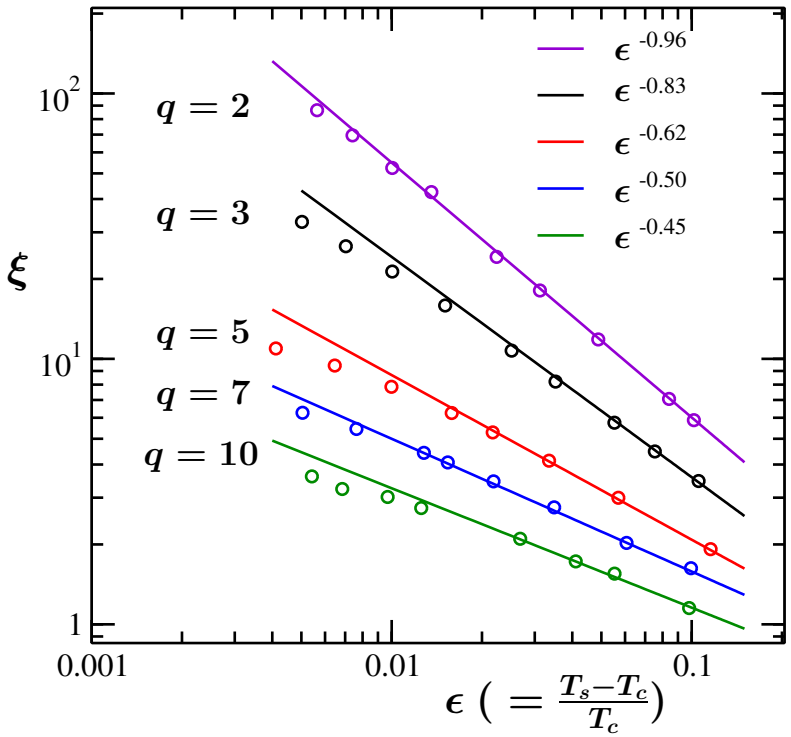

Figure 3.8: Correlation length, ξ, is plotted as a function of reduced temperature ϵ. The solid lines are fits to the simulation data, which have been shown by the open circles. Results from several values of q are included.

3.4 Kinetics of Ordering: A Short Discussion on the Scaling of Correlation Function

In non-conserved order-parameter (NCOP) dynamics of the Ising model, following quench inside the ferromagnetic region, the correlation function, $C(r,t)$, is well described by the Ohta-Jasnow-Kawasaki (OJK) function [27, 28]

$$C(r,t) = \frac{2}{\pi}\ \sin^{-1}\left[\ \exp\left(\frac{r^a}{8Dt}\right)\right], \tag{3.8}$$

where $a = 2$ and D is a diffusion constant. This, of course, complies with the growth behaviour [15, 16, 29]

$$\ell \sim t^{\alpha}; \quad \alpha = 1/2. \tag{3.9}$$

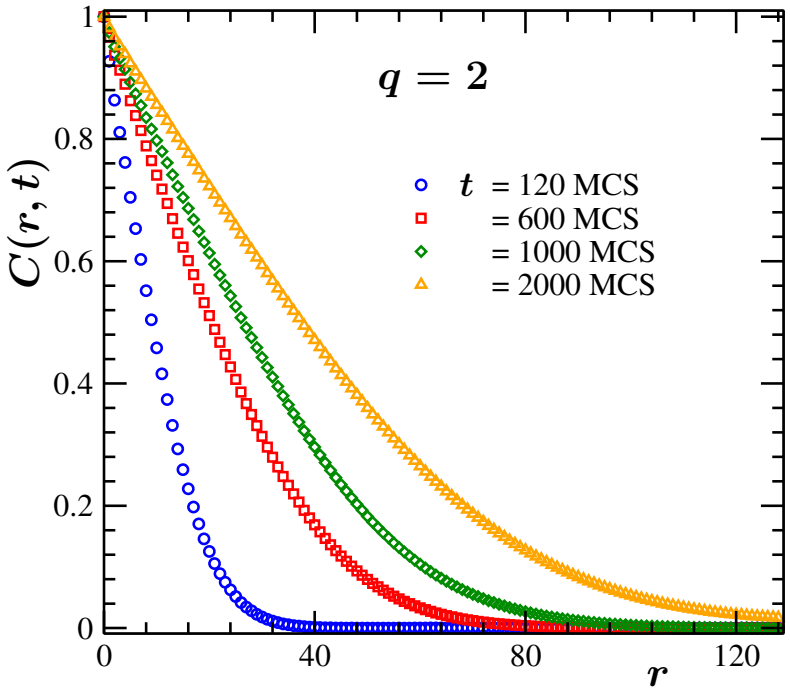

Figure 3.9: Plots of the decay of the correlation function, C(r,t), with the variation of the scalar distance r, for the mentioned time instances t in units of MCS. These results are for $q = 2$, following quenches from $T_s = \infty$ to $T_l = 0.5\,T_c$.

Fig. 3.9 shows the decay of $C(r,t)$ at different times during the evolution of a 2-state Potts system with Glauber spin-flip kinetics. Each of the systems discussed in this section have been quenched from temperature $T_s = \infty$ to temperature $T_l = 0.5\,T_c$.

On scaling the distance variable r, along abscissa, by the average domain size $\ell(t)$ of the systems corresponding to times t, we obtain a nice collapse of the data as shown in Fig. 3.10a. This implies self-similarity of pattern at different times [15]. The scaled data are in good agreement with the OJK function. However, we observed gradual deviation from the OJK function with the variation in q. In Fig. 3.10b we show a comparison of the scaled simulation data with the OJK function for $q = 10$. Such deviation is not unexpected because of the possibility of formation of point defects for $q > 2$. Important point to note is that there exists scaling.

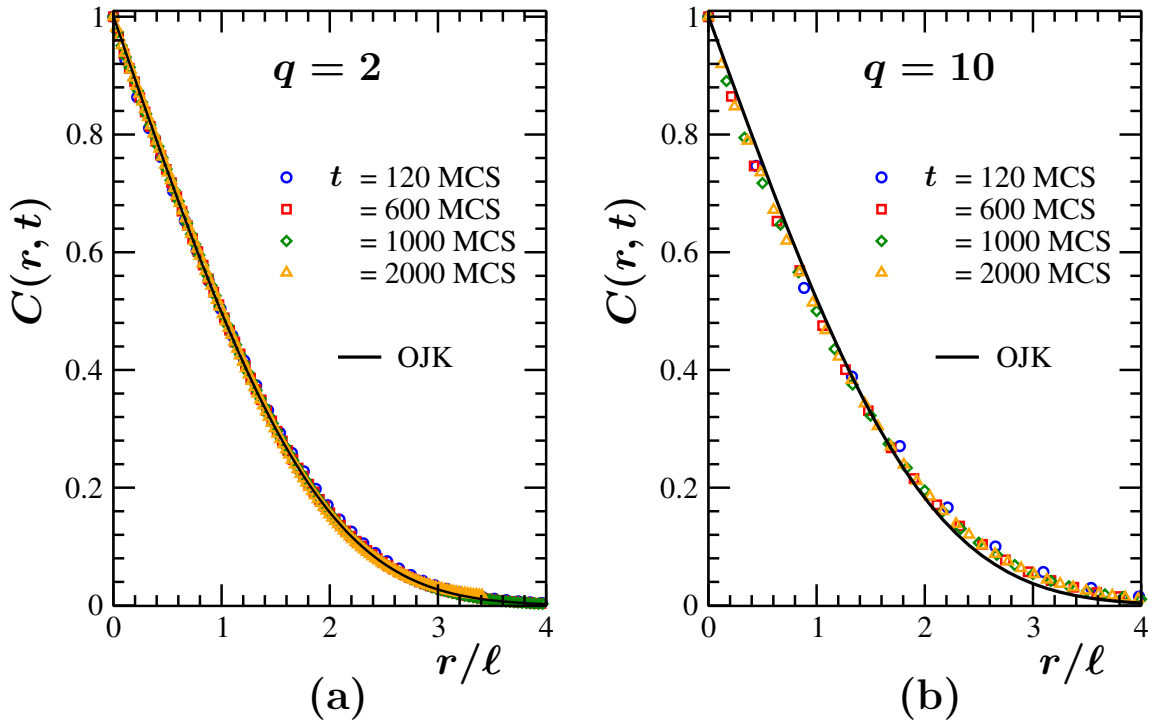

Figure 3.10: Scaling plots of $C(r,t)$ for (a) $q = 2$, using data presented in Fig 3.9 and (b) $q = 10$, for four different times. The solid line is the OJK function. While the scaled data for $q = 2$ is in good agreement with the OJK function, there is disagreement in the case of $q = 10$.

3.5 Mpemba Effect: Results and Discussions

We instantaneously quench the systems, prepared at different starting temperatures T_s, to the final lower temperature $T_l = 0.5\,T_c$. We present results by comparing the relaxations of hotter and colder systems in the cases of second-order, weakly first-order and first-order phase transitions.

The snapshots in Fig. 3.11 and 3.12, respectively, show evolutions of the 3 and 5-state Potts model for two different T_s values. It can be seen that the system at higher T_s reaches the final equilibrium state faster. The difference in the initial structures of the systems, in terms of the characteristic length, can be observed from Fig. 3.5, where the presence of higher spatial correlations in the systems at T_s nearest to T_c is easily identifiable.

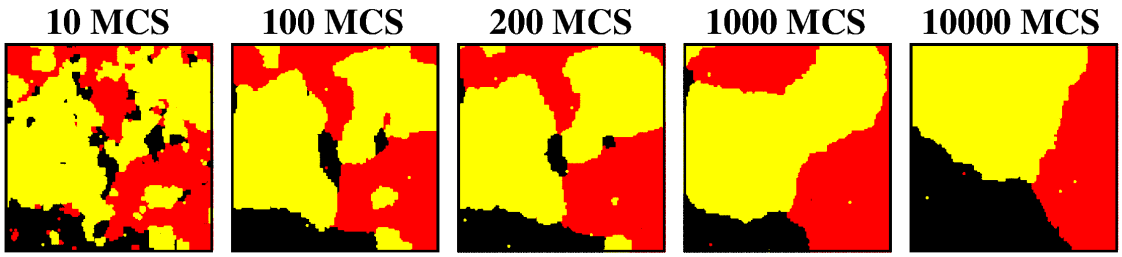

(a) Evolution snapshots at different times of a system initially at $T_s = 1.0$.

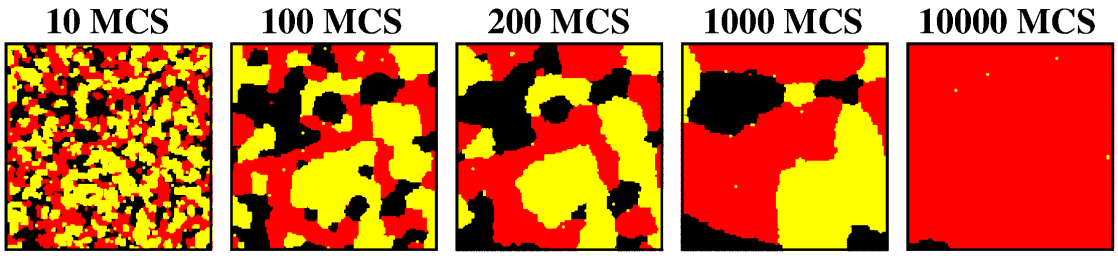

(b) Evolution snapshots at different times of a system initially at $T_s = 2.0$.

Figure 3.11: Snapshots from Monte Carlo simulations of the 3-state Potts model with Glauber dynamics following quenches to $T_l = 0.5\,T_c$. Different colours identify different states available in the system.

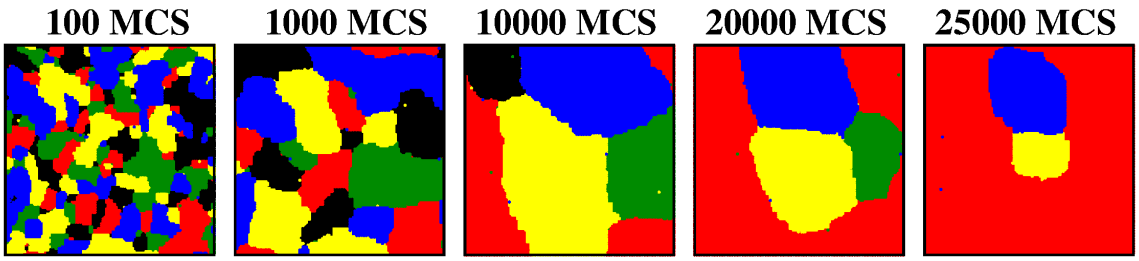

(a) Evolution snapshots at different times of a system initially at $T_s = 0.9$.

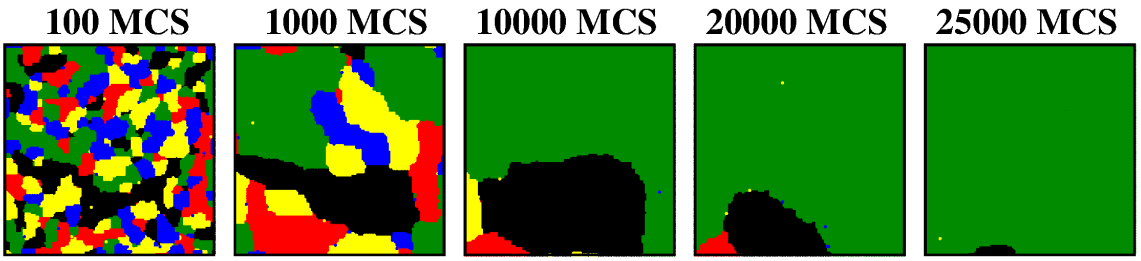

(b) Evolution snapshots at different times of the system initially at $T_s = 2.0$.

Figure 3.12: Snapshots from Monte Carlo simulations of the 5-state Potts model with Glauber dynamics, following quenches to $T_l = 0.5\,T_c$. Different colours identify different states available in the system.

3-state Potts model (Second-order Phase Transition):

In Fig. 3.13 we present, for $q = 3$, a plot of the decay of energy per spin, E, as a function of time, t, as the systems from different T_s relax towards the equilibrium at a common T_l, i.e., $T_l = 0.5\,T_c$. For the sake of clarity we split the plot into two halves, capturing the early and late time relaxations in the upper and and lower panels, respectively. It is clearly identifiable that the trend of energy decay in the lower panel is opposite to that of the upper panel. This indicates that there exists crossings among the curves, implying quicker decay of energy for higher T_s. This is the basic essence of the Mpemba effect. In order to demonstrate the early and late time behaviour more clearly, we take a reference potential energy value, E_{ref}, and note the time, $t_{c,E_{ref}}$, at which the energy curve for a T_s crosses E_{ref}.

We plot the variation of $t_{c,E_{ref}}$ over a set of T_s in Fig. 3.14a and Fig 3.14b to showcase the early and late time energy decay behaviours, respectively. The difference in the nature of the two plots at early and late times gives a clear indication of the presence of Mpemba effect.

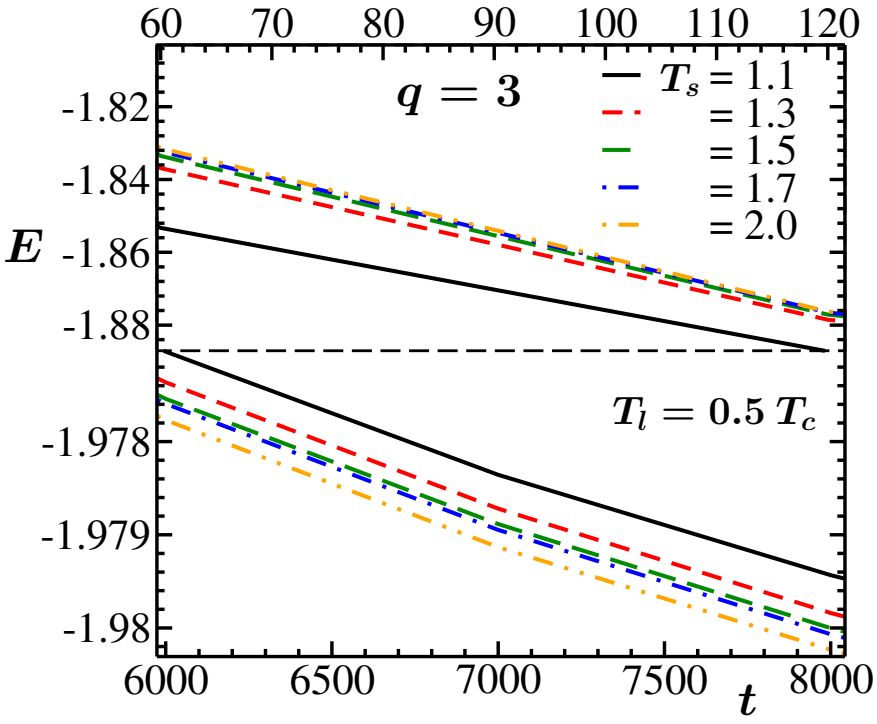

Figure 3.13: Energy per spin, E, is plotted versus time, t, for the $q = 3$ state Potts model. Results from several T_s values have been included. It is observed that the hotter system equilibrates faster. The frame has been split to capture the evolutions of the systems at early and late times simultaneously.

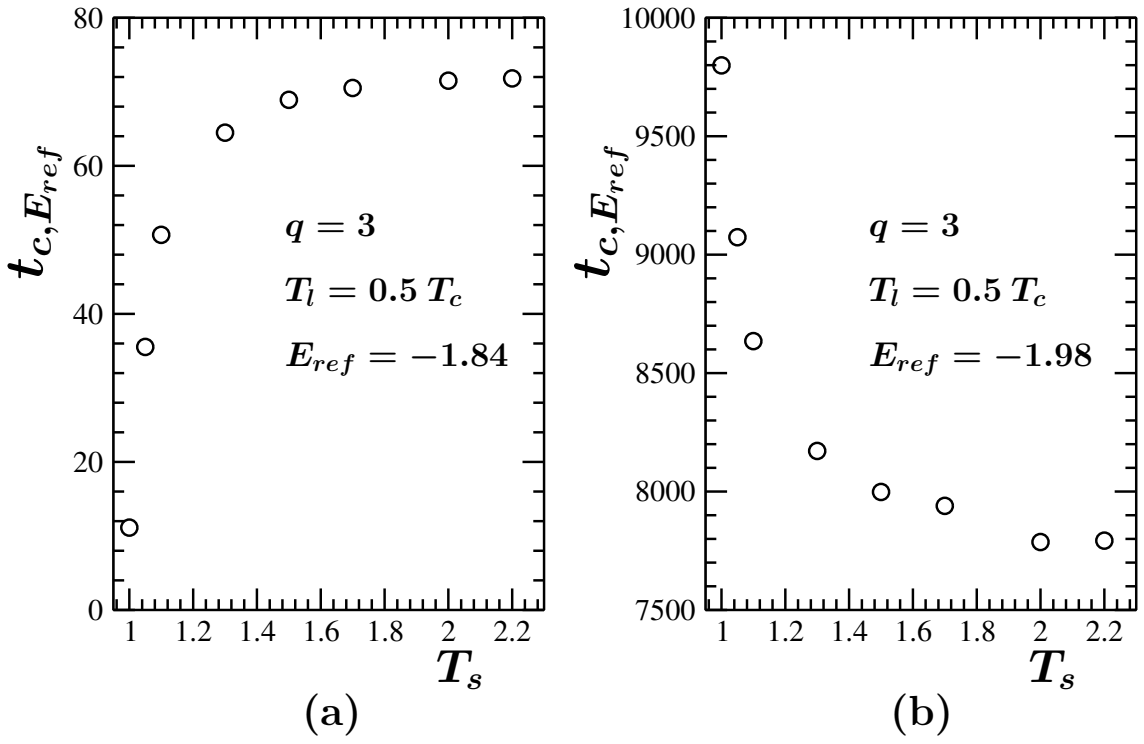

Figure 3.14: Plots of $t_{c,E_{ref}}$ versus T_s at (a) early and (b) late time regimes of evolution for $q = 3$. At late time regime, the time taken to reach E_{ref} monotonically decreases with the rise in T_s.

In Fig. 3.15, we show the times at which the energy curves of systems at different T_s are crossed or overtaken by the average energy curve of the systems starting from $T_s = \infty$. This crossing time is denoted as t_{c,E_∞}. The infinite temperature scenario is replicated by a system with a random initial configuration having "$\xi = 0$". All systems are seen to be overtaken by the $T_s = \infty$ energy curve.

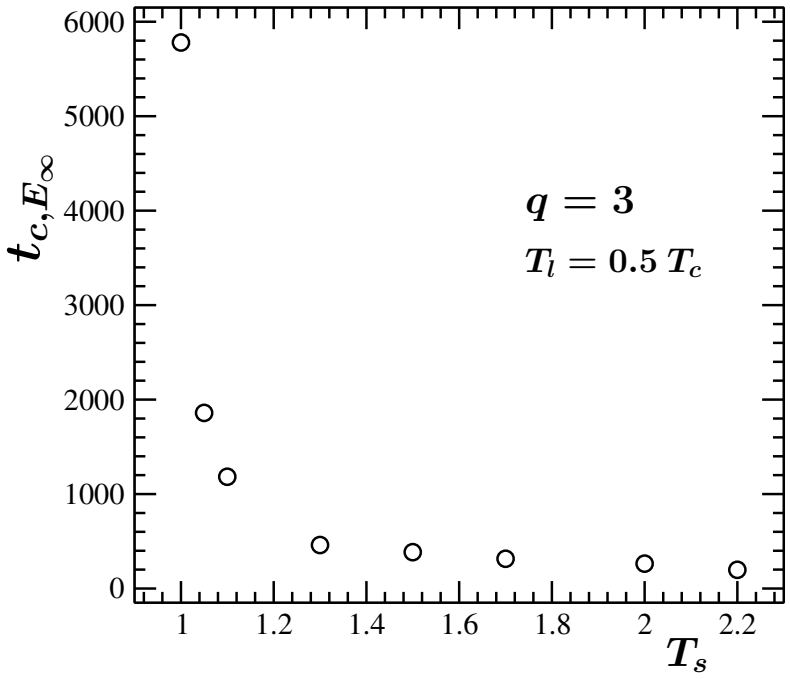

Figure 3.15: Plot of t_{c,E_∞} versus T_s for $q = 3$. See text for the definition of t_{c,E_∞}.

A similar trend of higher values of T_s relaxing faster, can be observed from the plots of average domain length, $\ell(t)$, versus time t, in Fig. 3.16, indicating again the presence of Mpemba effect. Crossings amongst the plots with different T_s values are clearly visible. In Fig. 3.17, we show the same plots of time dependence of average domain length $\ell(t)$ (Fig. 3.16) on a log-log scale. Here we also include the data for the systems starting from $T_s = \infty$. The initial differences in the average domain length values among the systems at different T_s, are clearly identifiable from these plots. The dashed line in the figure denotes a power-law growth with exponent 0.5. This power-law exponent of the domain growth holds good from reasonably early time for the cases of quench from $T_s = \infty$. However, for the systems with other T_s values this realization gets delayed.

During the early time the systems spend time in forgetting the initial correlations. While further studies are needed to make an accurate quantification of the memory loss period, the basic fact can be captured from the scaling plots of correlation functions below. At early times, because of the memory loss, one does not expect scaling in the

correlation functions. Given that for different T_s the value of ξ is different, during this transient period for different T_s the fractality will be different at a given instant. In fact the exhibition of Mpemba effect by the Potts model can be connected to the time dependence of memory loss. At very late times it is expected that the growth exponent $\alpha = 0.5$ will be followed by systems for all T_s. To validate that and make a meaningful conclusion on the Mpemba effect from the crossings of the length plot, it is desirable that $C(r,t)$ exhibits scaling asymptotically.

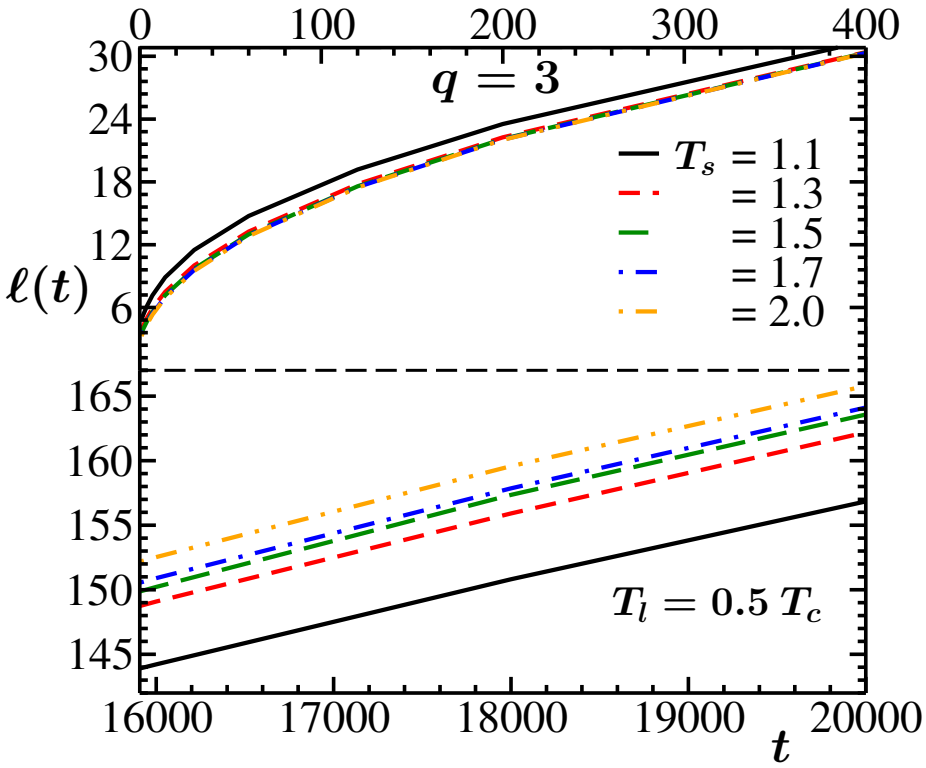

Figure 3.16: Plots of average domain length versus time for a range of T_s values for $q = 3$. The plots have been split into two frames for clearer views of early and late time regimes.

In Fig. 3.18, we plot the correlation function, $C(r,t)$, from different T_s, versus the scaled distance, r/ℓ, to show that the systems quenched from different T_s have structural similarities at least at late time and hence it is appropriate to compare their characteristic lengths [7]. Except for $T_s \approx T_c$ the systems at other T_s are seen to attain a good scaling at an early time. The overall scaling is seen to improve with the increase in time. Beyond the crossing regime, at around $t = 1000$ MCS, i.e., the time scale around which the crossings amongst majority of the systems have already occured, there is a good data collapse.

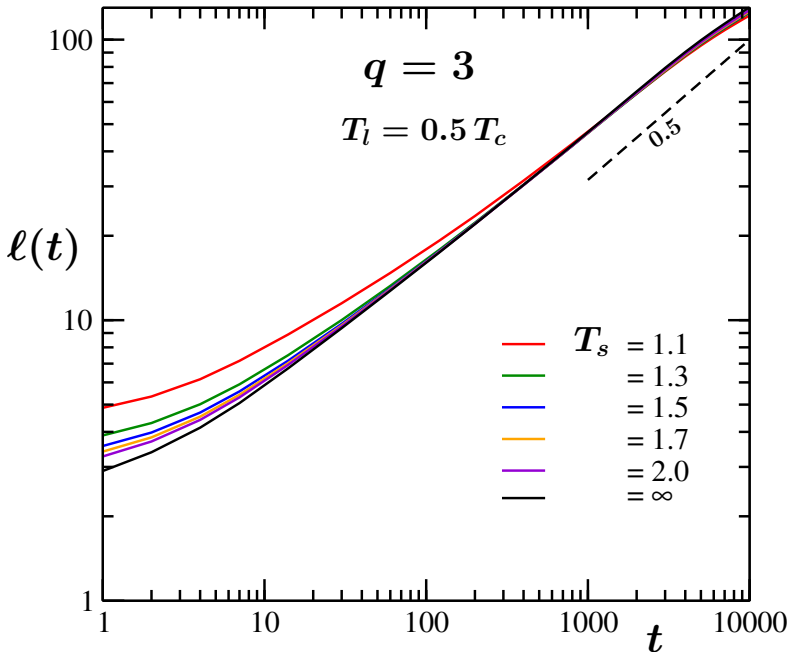

Figure 3.17: Plots of $\ell(t)$ versus t, for different T_s, on a log-log scale for $q = 3$. The dashed line denotes a power-law growth behaviour with exponent 0.5.

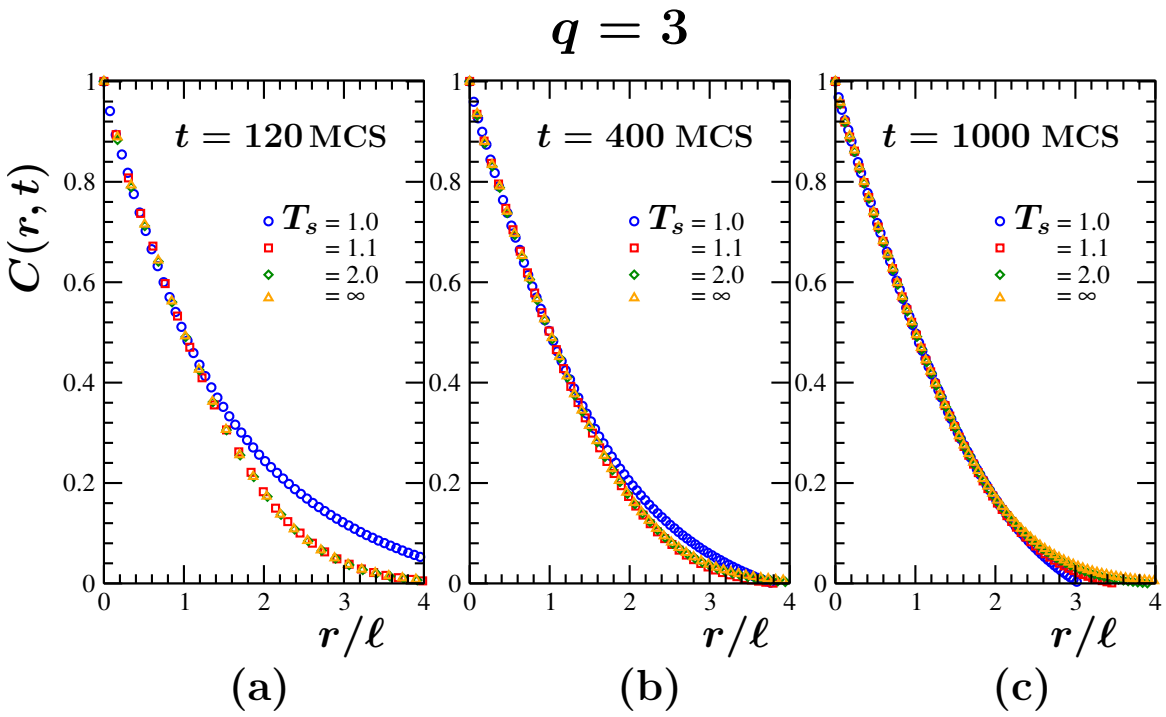

Figure 3.18: Scaled correlation function, for $q = 3$, at times (a) $t = 120$ MCS, much before the crossings; (b) $t = 400$ MCS; and (c) $t = 1000$ MCS, in or beyond the crossing regime.

5-state Potts model (Weak First-order Phase Transition):

In Fig. 3.19, we show the time dependence of potential energy. As observed in the case of $q = 3$, in this case too there is a faster decay of energy for the systems having higher T_s. The early and late time behaviours are shown in Fig. 3.20a and 3.20b, respectively, by plotting the times of crossing different reference energy values by energy curves corresponding to different T_s. We also plot t_{c,E_∞} as a function of T_s in Fig. 3.21. We further show the growth of average domain length in the systems as a function of time t in linear (Fig. 3.22) and log-log (Fig. 3.23) scales. In Fig. 3.23, it is seen that at late time, following crossings, all the data sets with different T_s are growing in a power-law fashion. Overall, the picture is same as in the case of $q = 3$. These trends indicate the presence of Mpemba-like behaviour in the 5-state Potts model having weak first-order transitions [12].

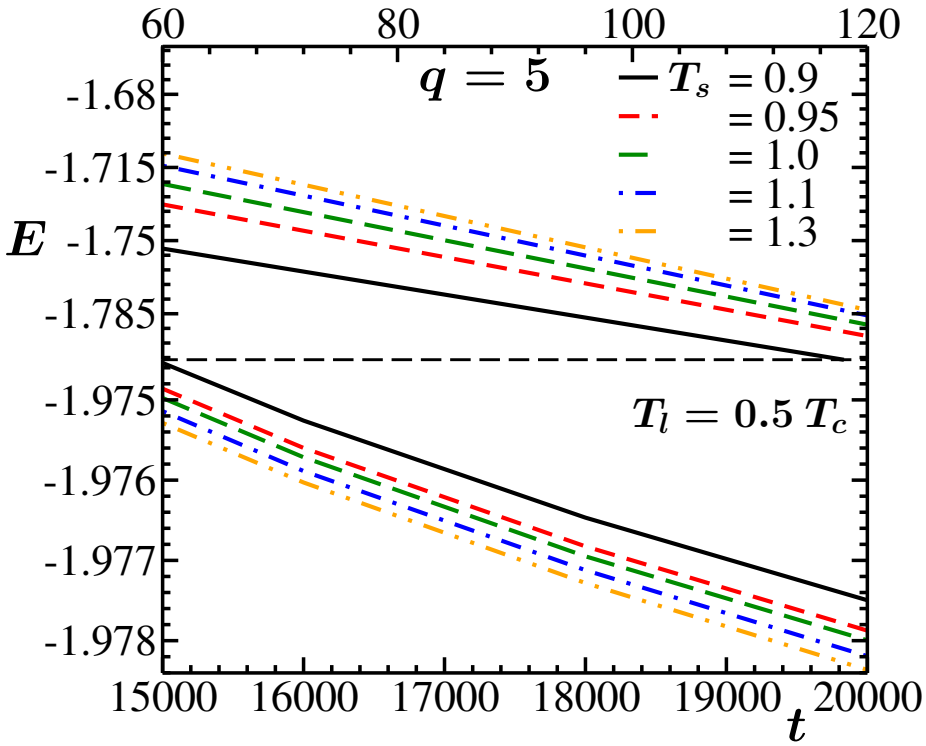

Figure 3.19: Energy per spin, E, versus time, t, for the $q = 5$ state Potts model. Results from several T_s values have been plotted. The upper and lower frames capture energy decay at early and late times, respectively.

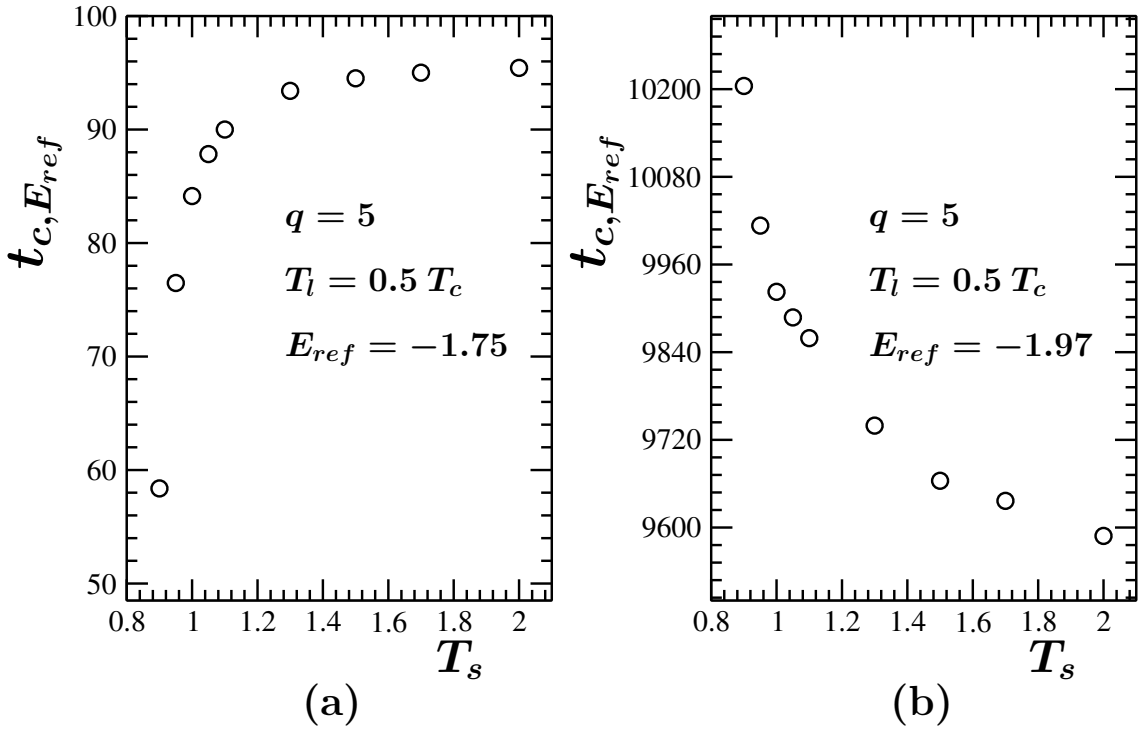

Figure 3.20: Plots of $t_{c,E_{\rm ref}}$ versus T_s at (a) early and (b) late time regimes of evolutions for $q = 5$.

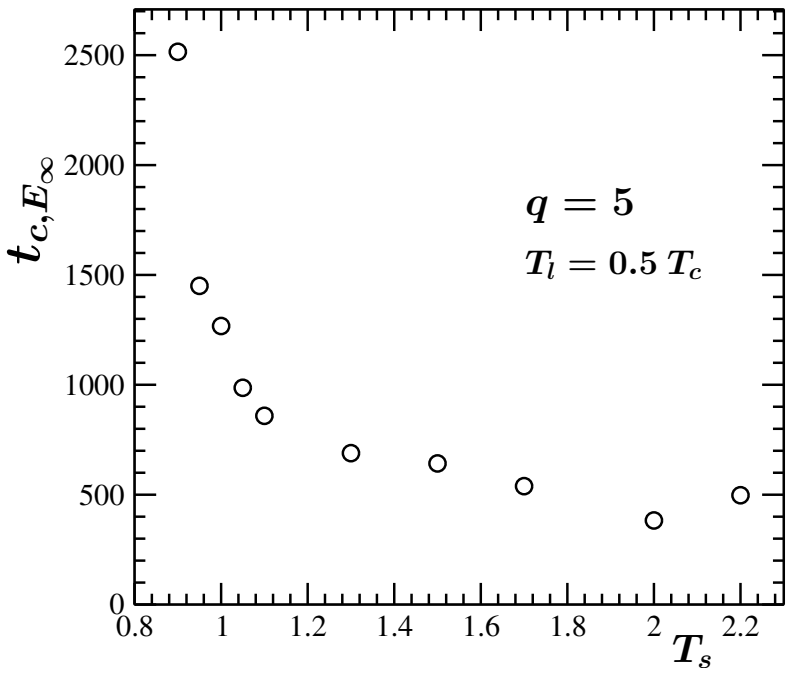

Figure 3.21: Plot of t_{c,E_∞} versus T_s for $q = 5$. The value of t_{c,E_∞} decreases monotonically with the increase in T_s.

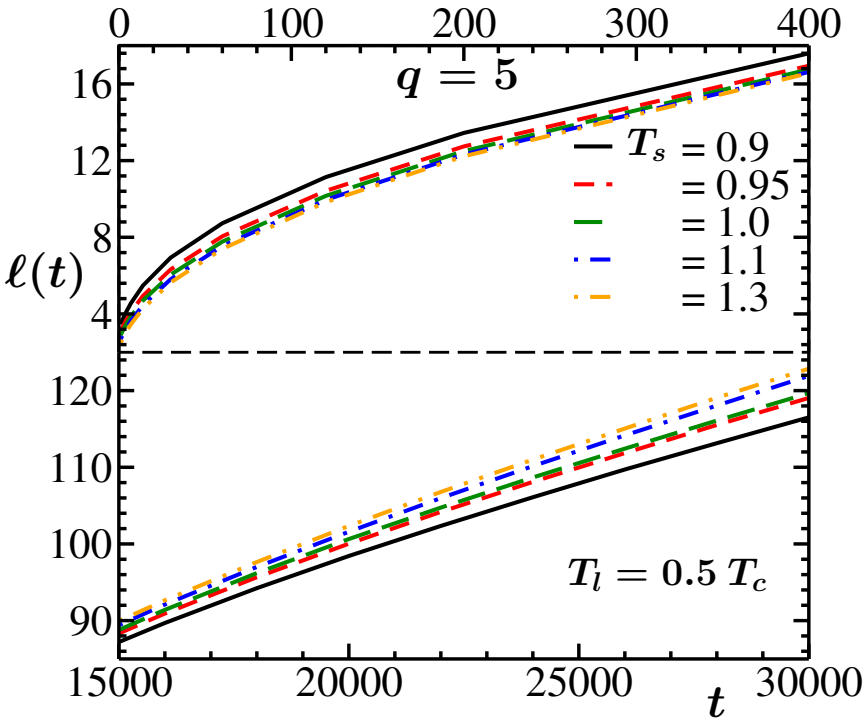

Figure 3.22: Plots of average domain length versus time for a range of T_s values for $q = 5$. The plots have been split to help view the early and late time regimes clearly.

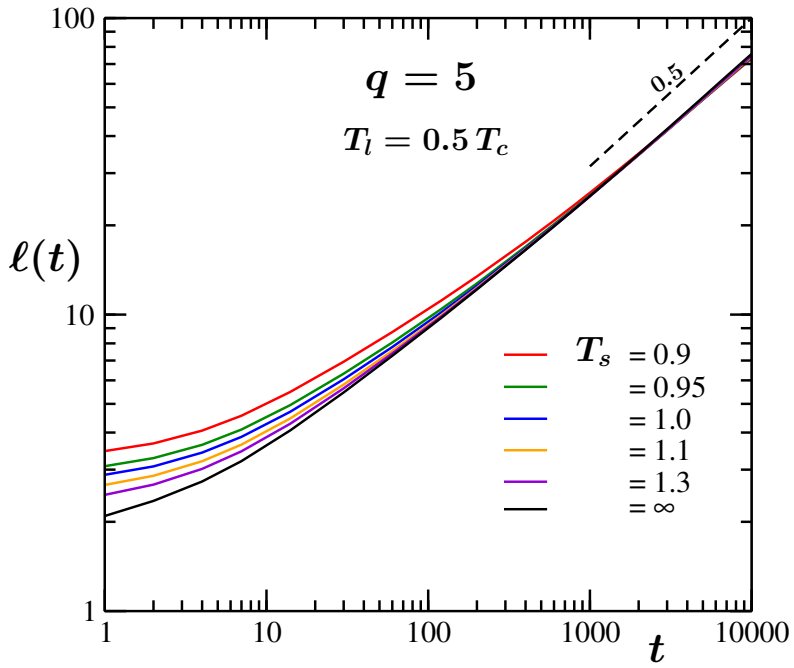

Figure 3.23: Plots of $\ell(t)$ versus t on a log-log scale for $q = 5$. Results from several T_s values have been shown. The dashed line denotes a power-law growth behaviour with exponent 0.5.

We plot the scaled correlation functions for different temperatures at time scales ranging from very early (Fig. 3.24) to early (Fig. 3.25a, 3.25b) to the late time (Fig. 3.26a, 3.26b) regimes. The correlation function $C(r,t)$ is seen to scale reasonably well at an early time of $t = 30$ MCS. However, at an even early time of $t = 7$ MCS, the variation in the morphology of the systems for different T_s can be seen from Fig. 3.24. At very early times the scenario of scaling is somewhat different. Close to T_c, the systems have fractal-like structures. For such systems, the correlation function scales as [22, 30–32]

$$C(r,t) \equiv r^{d-d_f}\, \widetilde{C}(r/\ell(t)), \tag{3.10}$$

where d and d_f are the dimensions of space and fractal, respectively. Nevertheless, these fractal-like features disappear later and we obtain good scaling with $d = d_f$ at times considerably before the crossings start [7]. This scaling continues till late time.

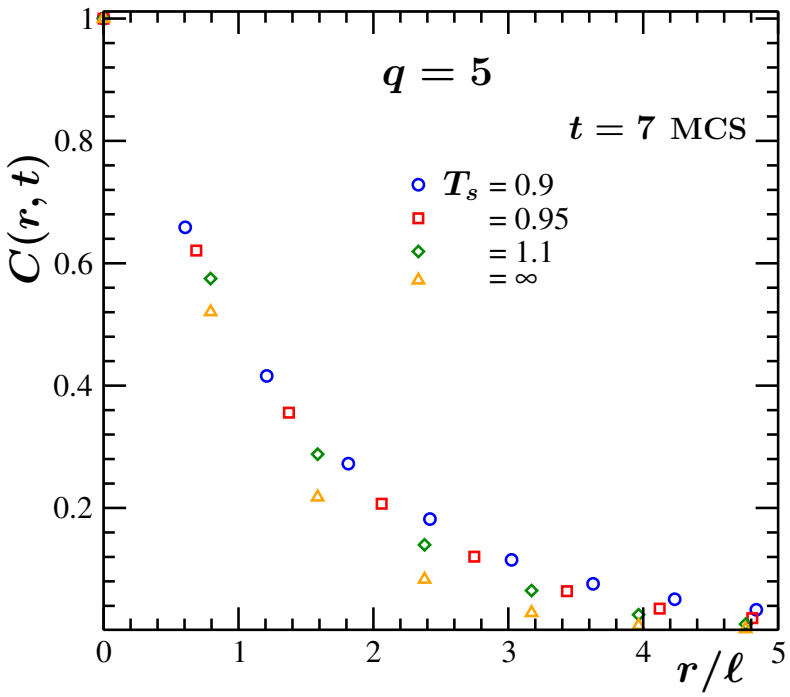

Figure 3.24: Scaled correlation functions at $t = 7$ MCS, for $q = 5$. The structures of the systems for different T_s are not self-similar.

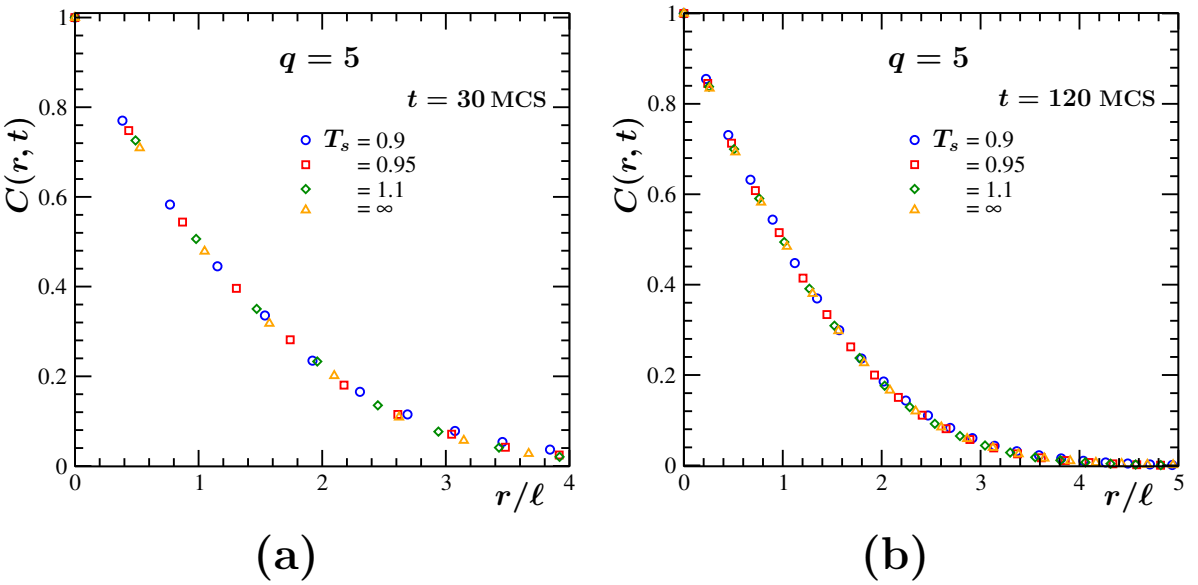

Figure 3.25: Scaled correlation functions at (a) $t = 30$ MCS and (b) $t = 120$ MCS, for $q = 5$.

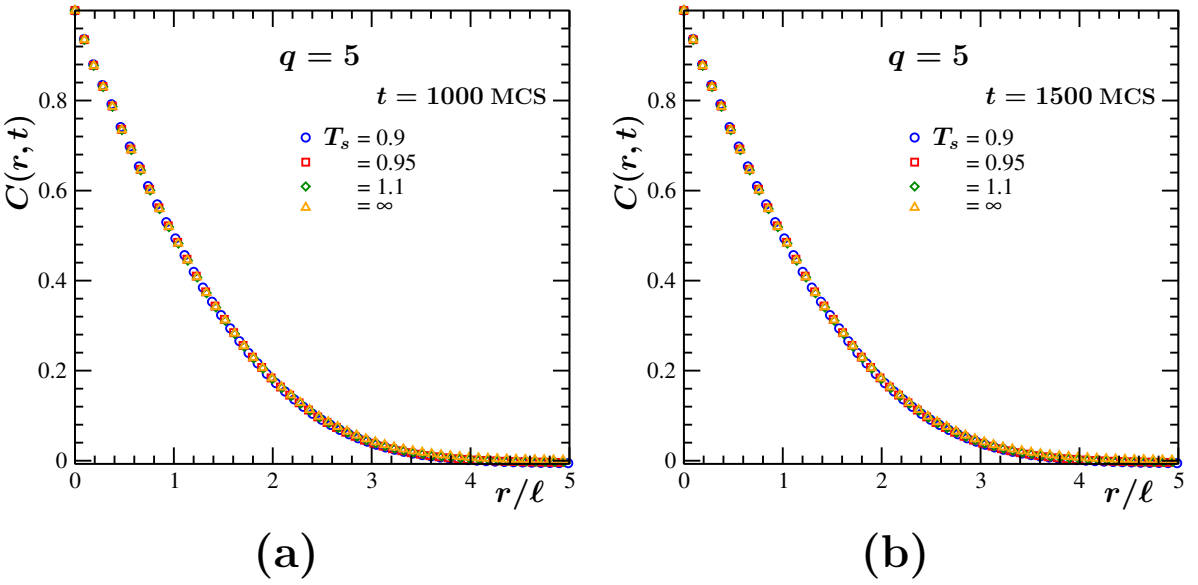

Figure 3.26: Scaled correlation functions at (a) $t = 1000$ MCS and (b) $t = 1500$ MCS, for $q = 5$, in the crossing regime. Data from different T_s show "perfect" scaling.

7 and 10-state Potts model (First-order Phase Transitions):

Parallel to the results in the cases of $q = 3$ and $q = 5$, we observe Mpemba Effect for $q = 7$ and $q = 10$ as well. However, the general observation is that with the increase of q the crossing time gets delayed. This is because the enhancement in the equilibrium correlation length is weaker, with approach to T_c, as q becomes larger.

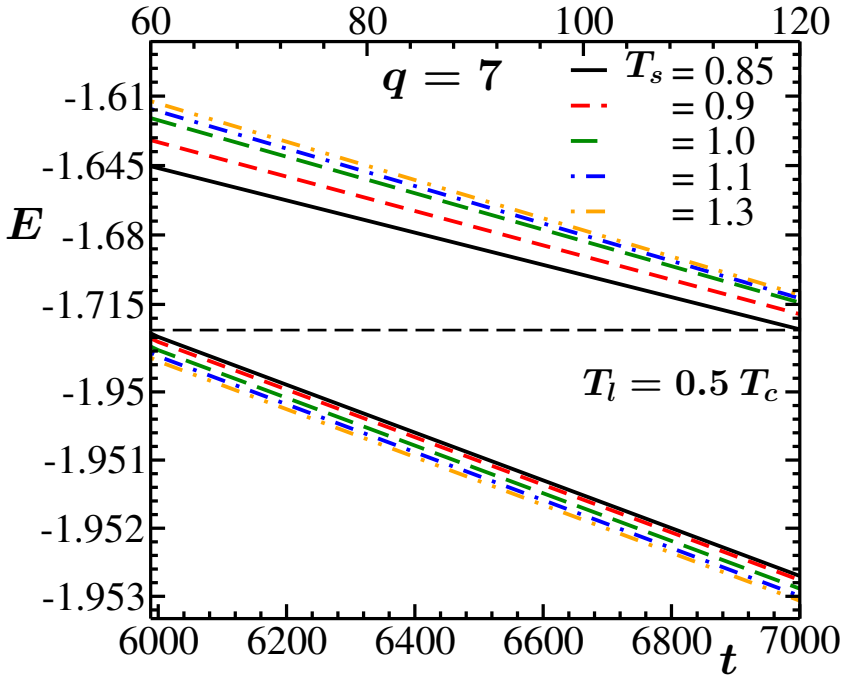

(a) 7-state Potts model.

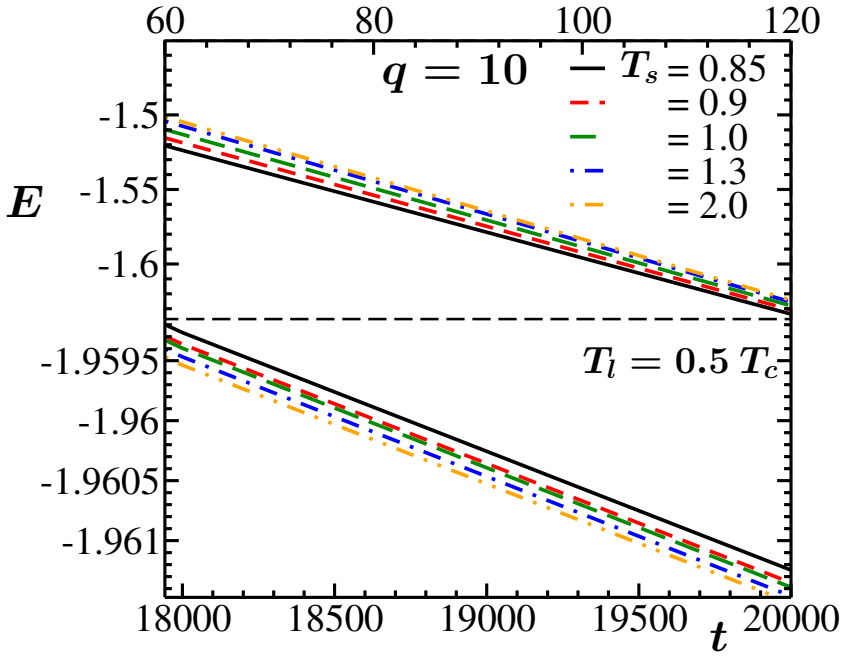

(b) 10-state Potts model.

Figure 3.27: Energy per spin, E, versus time, t, for the (a) $q = 7$ and (b) $q = 10$ state Potts models. The frames have been split for clear visibility of the relaxation trends at early and late times simultaneously. Data from several T_s values have been included.

In Fig. 3.27, we present the behaviour of relaxations of the systems by plotting the energy per spin, E, as a function of time, t, Fig. 3.27a and Fig. 3.27b containing the results for $q = 7$ and $q = 10$, respectively. Next we show the early (Fig. 3.28) and late (Fig. 3.29) time crossings of energy curves, for both the q values, with fixed energy values. We further plot t_{c,E_∞} versus T_s in Fig. 3.30. We plot the average domain length as a function of time t in linear (Fig. 3.31) and log-log (Fig. 3.32) scales. Closer views of the results in Fig. 3.32 tell that the late time exponent of the power-law behaviour is somewhat less than the usual 0.5 exponent. Such a reduction in the growth exponent was also reported in previous works [33–36]. We plot the scaled $C(r, t)$ from different times (MCS) for the 7 and 10-state Potts model in Fig. 3.33 and Fig. 3.34, respectively. All these observations imply the presence of Mpemba-like behaviour in the 7-state and 10-state Potts model with first-order phase transitions. However, as already stated, reasonably good scaling of the correlation functions for different T_s from rather early time and increase in crossing times imply that the effect is less prominent and may disappear for very large q.

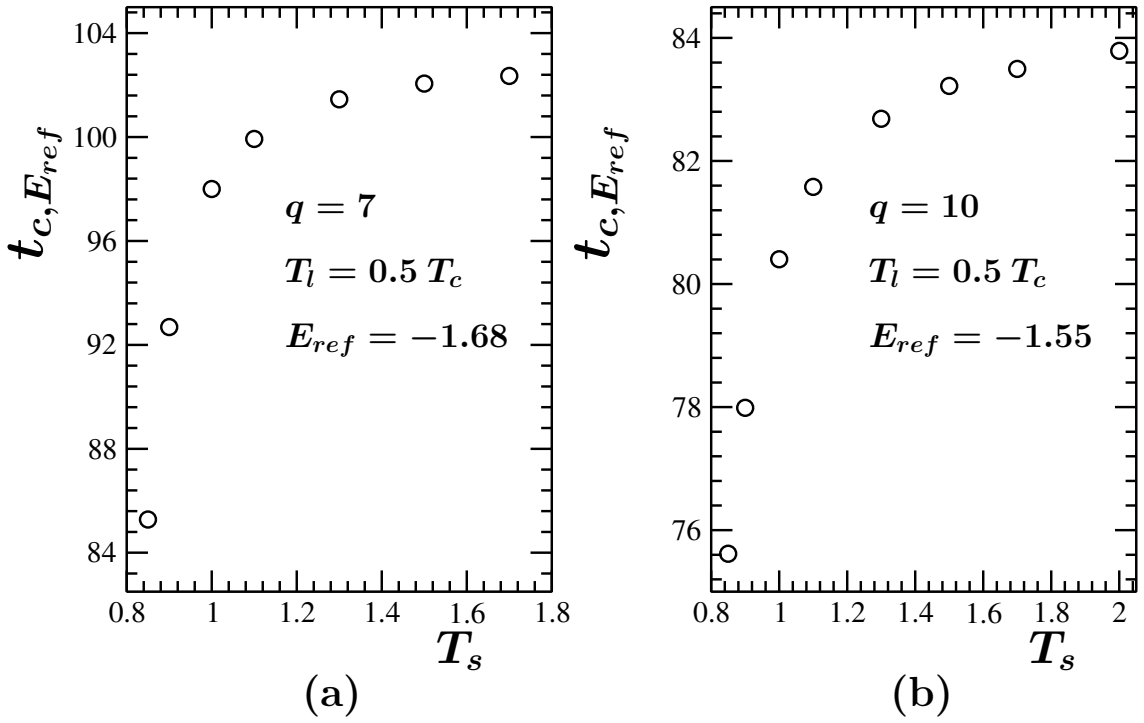

Figure 3.28: Plots of $t_{c,E_{ref}}$ versus T_s in early time regimes of evolutions for (a) $q = 7$ and (b) $q = 10$.

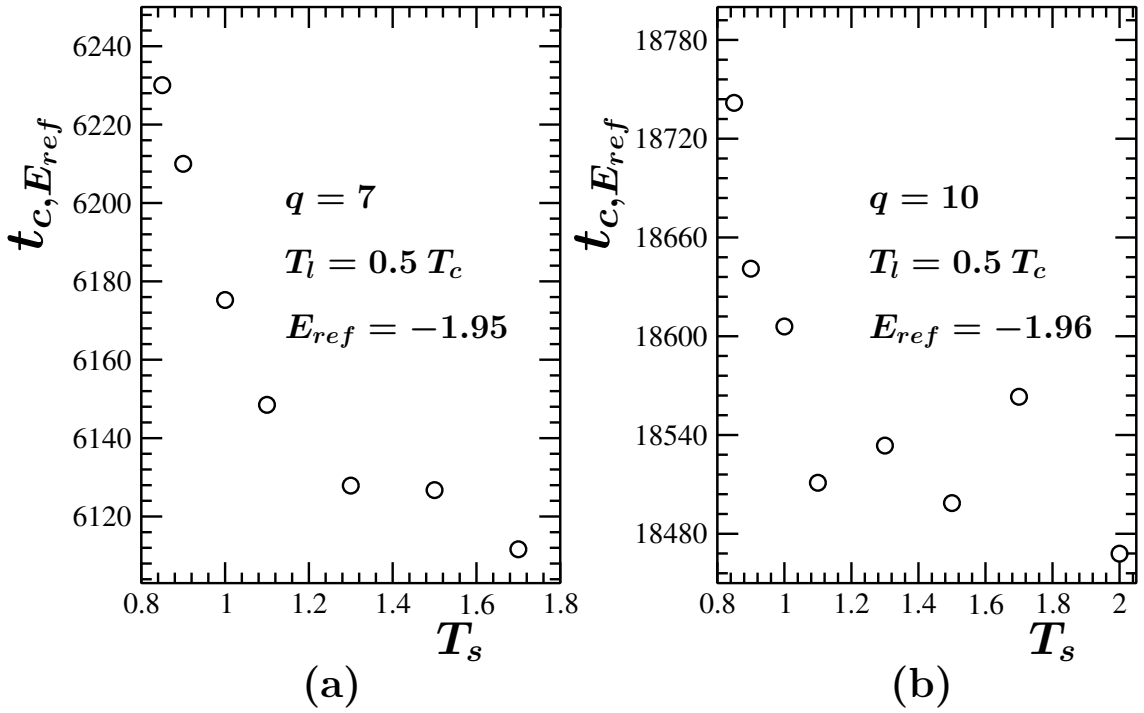

Figure 3.29: Plots of $t_{c,E_{ref}}$ versus T_s in late time regimes of evolutions for (a) $q = 7$ and (b) $q = 10$.

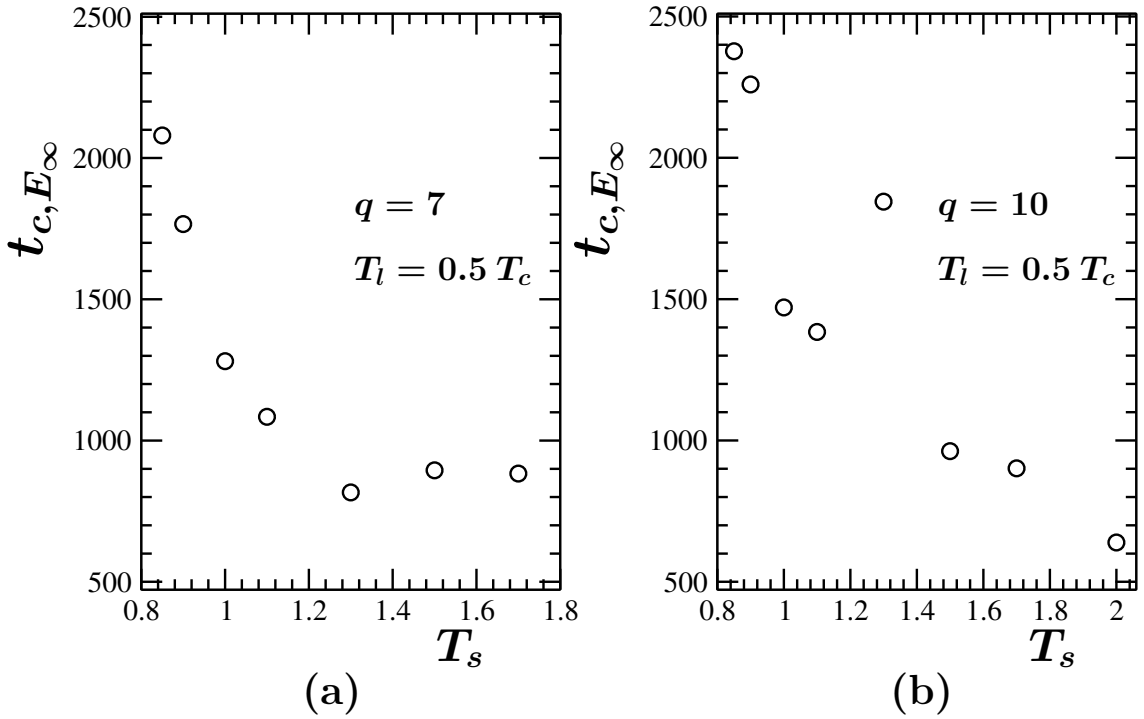

Figure 3.30: Plots of t_{c,E_∞} versus T_s for (a) 7-state and (b) 10-state Potts model.

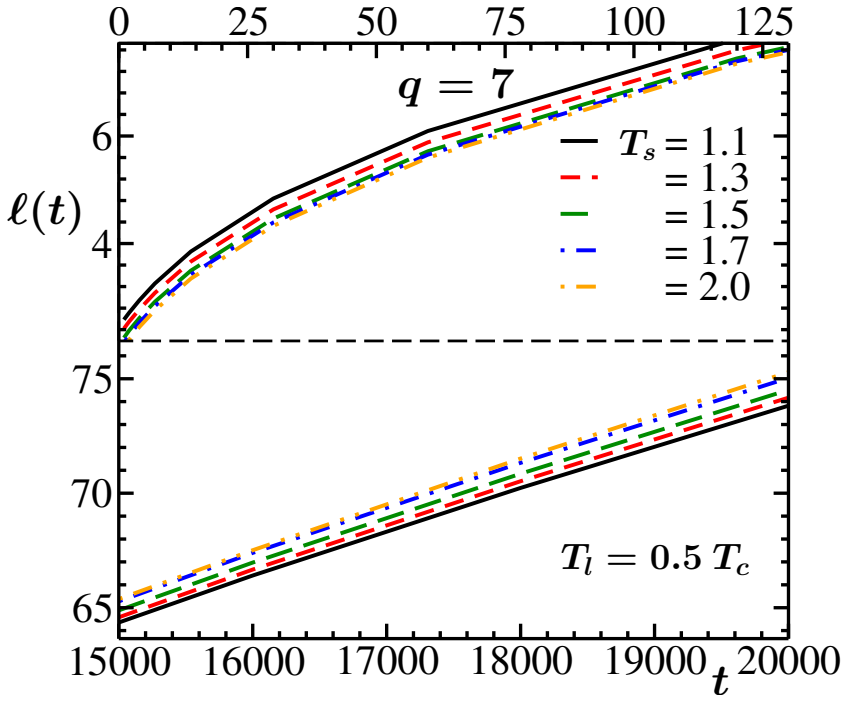

(a) 7-state Potts model.

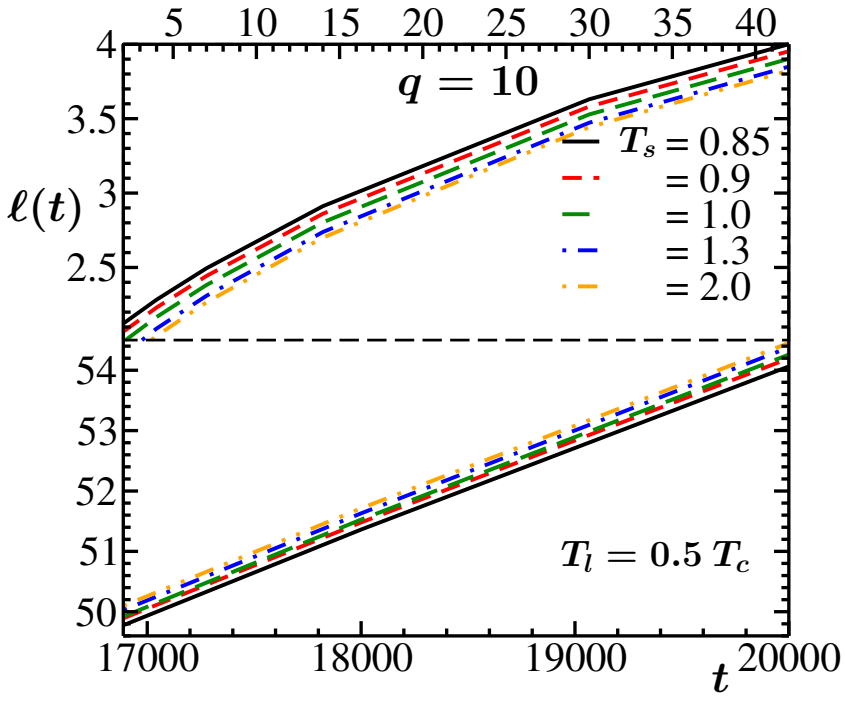

(b) 10-state Potts model.

Figure 3.31: Plots of average domain length versus time for a range of T_s values, for (a) $q = 7$ and (b) $q = 10$. The plot has been split to help view the early and late time regimes clearly.

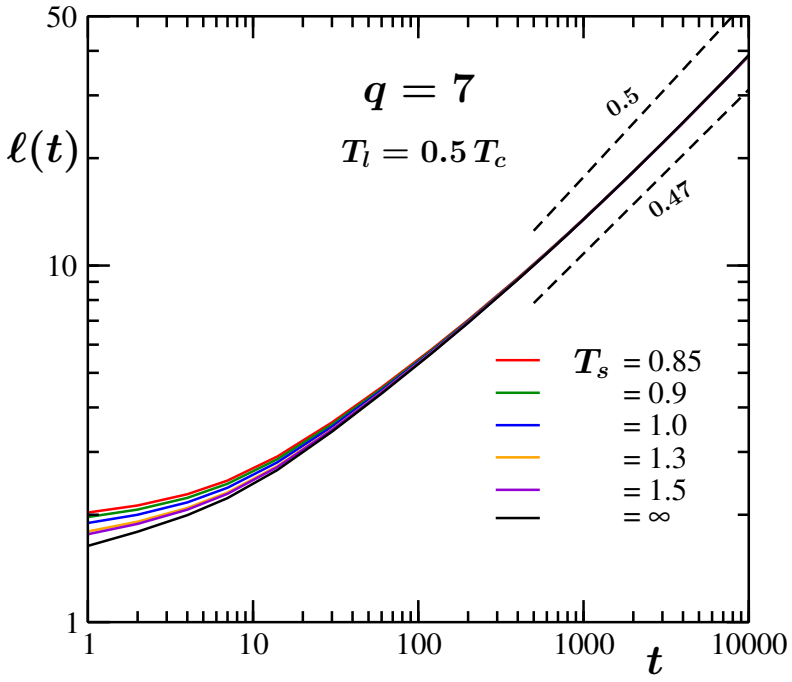

(a) 7-state Potts model.

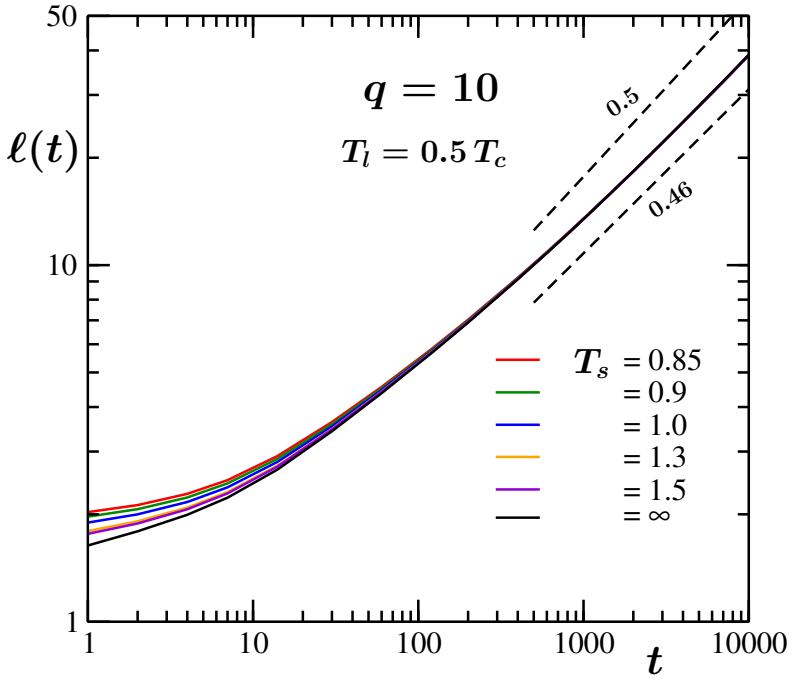

(b) 10-state Potts model.

Figure 3.32: Plots of $\ell(t)$ versus t on a log-log scale for (a) $q = 7$ and (b) $q = 10$. The dashed lines denote power-law growths. Data from several T_s values have been included for each of the q values.

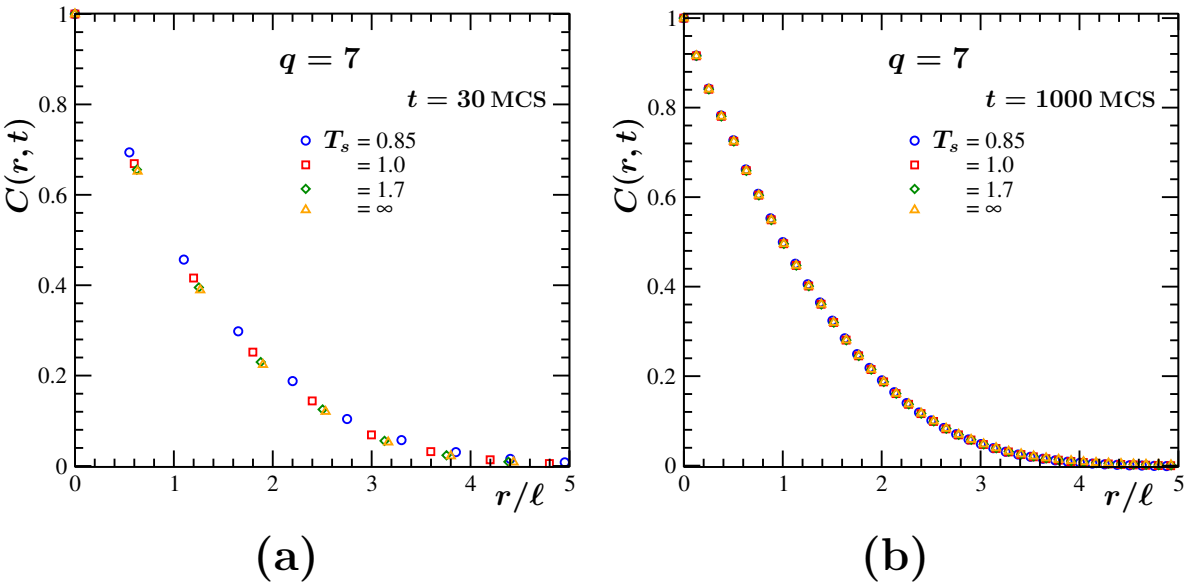

Figure 3.33: Scaled correlation functions at (a) early and (b) late times, for $q = 7$.

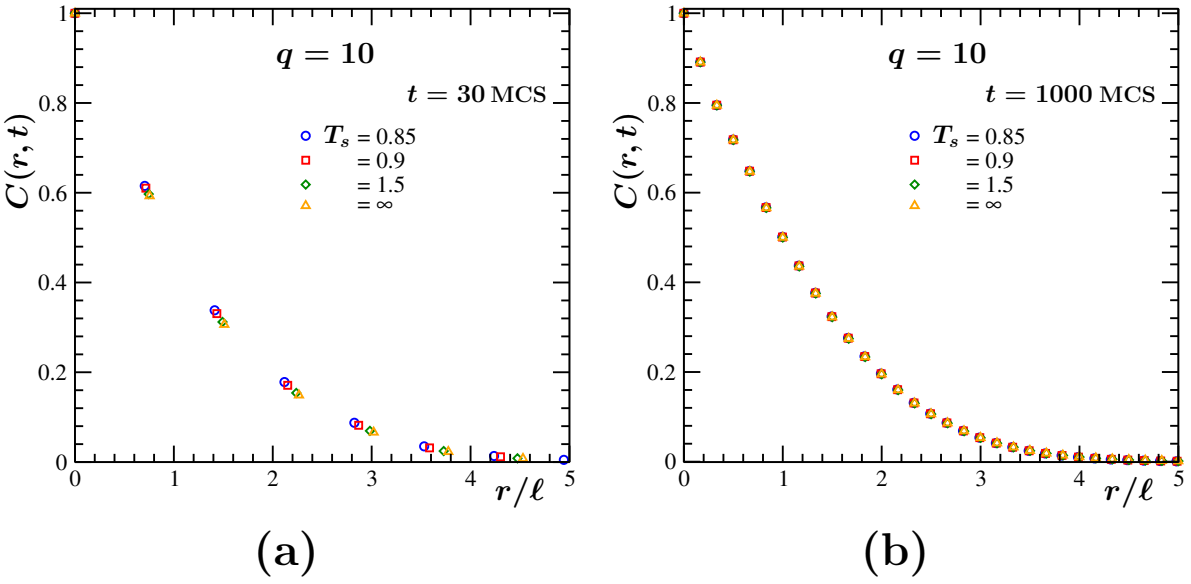

Figure 3.34: Scaled correlation function at (a) early and (b) late times, for $q = 10$, using data from different T_s values.

3.6 Summary and Conclusion

We have studied kinetics of phase transitions in q-state Potts model [8–13]. The objective has been to investigate the Mpemba effect [1–7]. Keeping this purpose in mind we have prepared initial configurations at various different starting temperatures (T_s) above the critical temperatures T_c. These configurations are quenched to the temperature $T_l = 0.5\,T_c$.

We have considered several values of q, viz., $q = 3, 5, 7$ and 10. For $q = 3$, the model exhibits a second-order transition [8–14]. For $q = 5$ there exists a weak first-order transition [12]. Standard first-order transitions [8–14] are expected for $q = 7$ and 10. Our conjecture is that enhancement in the spatial correlation (ξ), as T_s approaches T_c, is responsible for the exhibition of Mpemba effect in this model. In the case of first-order transition, a divergence of ξ, on approach of T_s to T_c, is not expected. However, a continuous increase in ξ may occur towards a constant value. If this is so, it is possible that the Mpemba effect will be observed for both types of transition.

Mpemba effect is related to the faster equilibration of a system starting from a higher temperature than the colder ones when quenched to a common lower temperature. At higher temperatures the potential energy is higher. Thus, we expect crossings in the plots of energy decay for systems starting from different T_s values. This was indeed observed for all the considered q values. Such crossings are expected in the plots of time dependence of characteristic length scale as well.

Note that the equilibrium structures at different T_s have fractal character [22]. During the early periods of evolution, following quenches to the ferromagnetic regime, the systems try to forget the memory of such fractal structure. Because of this, the "standard self-similarity" should be missing during this transient period. However, at late times, structures from different T_s should obey same functional form. This, indeed, we have observed which makes our conclusion on the presence of Mpemba effect meaningful.

The Mpemba effect in such spin systems may be a result of the competition between the pace of memory loss and the rate of scaling growth. Because of larger ξ at lower T_s, the nonequilibrium length plots start in reverse order. If the memory has a slower decay rate than the asymptotic scaling growth rate, it is possible that there will be crossings. To make a concrete statement on this memory related matter more systematic studies are needed that should be supported by very accurate data and advanced methods of analysis.

We have observed the effect for second as well as first-order transitions. A first-order transition provides two possibilities: i) far away from T_c, ξ increases and then practically saturates before T_s reaching T_c and, as mentioned above, ii) ξ keeps growing, to a constant value, until T_c is reached. We have calculated ξ quite close to T_c for all the q values. Within the considered temperature ranges we have not observed any perfect plateauing of this quantity. Approaching even closer to T_c will generate results that may not be sensitive to temperature, particularly for large q values. In any case, over the studied ranges of temperature, ξ showed detectable enhancement and Mpemba effect was observed for all the q values. However, we warn that for much larger values of q the effect may not be clearly observed.

We have made further interesting observations. We make only a brief mention of these outcomes from preliminary studies. These are related to certain differences when quenches are performed to different final temperatures. In Fig. 3.35 we show plots of $t_{c,E_{ref}}$ versus T_s, for $q = 3$. There we have compared the results from $T_l = 0$ and $0.5\,T_c$. Clearly, the trends are different for T_s close to T_c. For $T_l = 0$, the data set implies that the Mpemba effect may not be observed for T_s very close to T_c, even for a second-order transition.

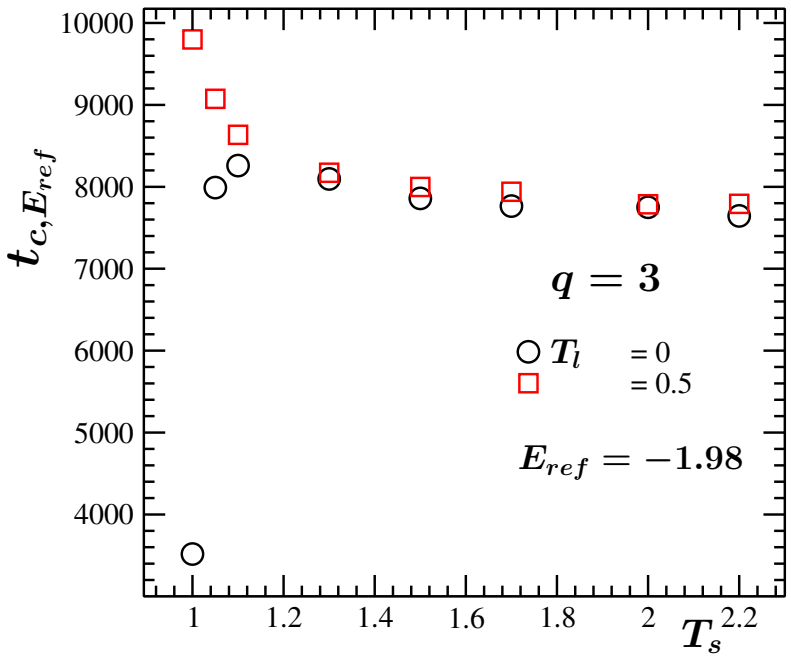

Figure 3.35: Plots of $t_{c,E_{ref}}$ versus T_s for quenches to $T_l = 0$ and $T_l = 0.5\,T_c$, at late times, for $q = 3$. Systems from the temperature T_s that is nearest to T_c, attains the reference energy at the earliest for quenches to $T_l = 0$, which is opposite to the observation in the case of quench to $T = 0.5\,T_c$.

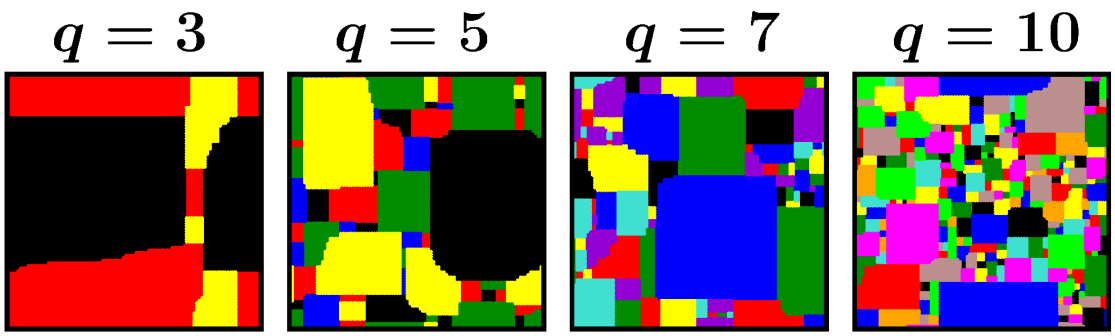

(a) Frozen snapshots for quenches from $T_s = \infty$ to $T_l = 0$.

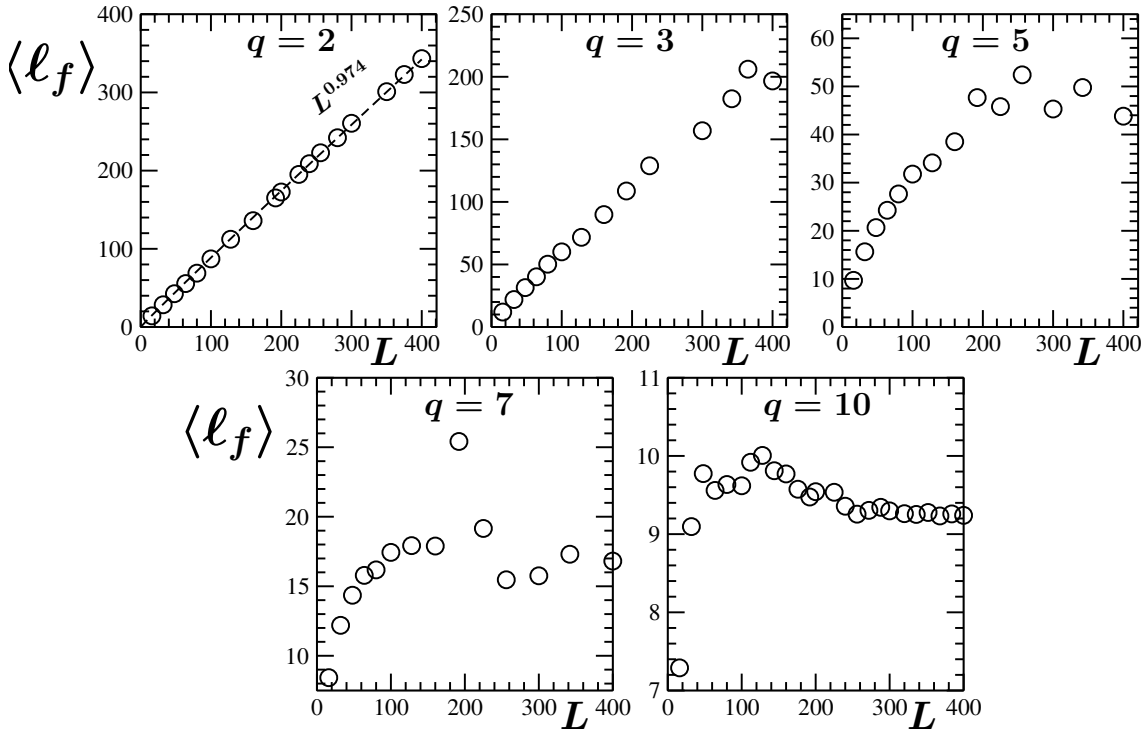

(b) Plots of $\langle \ell_f \rangle$ as a function of L, for quenches from $T_s = \infty$ to $T_l = 0$.

Figure 3.36: (a) Snapshots of frozen states for the mentioned q values. Sharp interfaces that are formed during coarsening suppress curvature driven domain growth. (b) Variation of the average final domain length, $\langle \ell_f \rangle$, with the change in system size, L, for different q values. For $q = 2$, the plot is nearly linear, for $q > 2$ there is deviation from linearity. For $q = 7$ and $q = 10$, $\langle \ell_f \rangle$ is seen to saturate and become independent of L.

In certain other systems it is thought that frustrations or metastability is the reason behind the presence of Mpemba effect [5]. Such metastability occurs in the cases of

Ising [37, 38] and Potts model [39, 40] as well. In Fig. 3.36a we show some snapshots of metastable configurations for different q values following quenches from $T_s = \infty$ to $T_l = 0$. In Fig. 3.36b we show plots of average final length $\langle \ell_f \rangle$ as a function of system sizes L, for different q values for the same quench protocol. For each of the q values, the results imply freezing. Expected ground states are not obtained. For high q values it is even more interesting. Beyond certain value of L, $\langle \ell_f \rangle$ appear constant. To check whether the results in Fig. 3.35 have bearing with such freezing, one needs to carry out more systematic study on this freezing aspect by varying T_s as well as T_l and simulating over much longer times. We leave this task for future.

References

[1] E.B. Mpemba and D.G. Osborne, Phys. Educ. **4**, 172–175 (1969).

[2] A. Lasanta, F.V. Reyes, A. Prados, and A. Santos, Phys. Rev. Lett. **119**, 148001 (2017).

[3] A. Torrente, M.A. López-Castaño, A. Lasanta, F.V. Reyes, A. Prados, and A. Santos, Phys.Rev. E **99**, 060901 (2019).

[4] A. Biswas, V.V. Prasad, O. Raz, and R. Rajesh Phys. Rev. E **102**, 012906.

[5] M. Baity-Jesi, E. Calore, A. Cruz, L.A. Fernandez, J.M. Gil-Narvión, A. Gordillo-Guerrero, D. Iñiguez, A. Lasanta, A. Maiorano, E. Marinari, V. Martin-Mayor, J. Moreno-Gordo, A.M. Sudupe, D. Navarro, G. Parisi, S. Perez-Gaviro, F. Ricci Tersenghi, J.J. Ruiz-Lorenzo, S.F. Schifano, B. Seoane, A. Tarancoń, R. Tripiccione, and D. Yllanes, Proc. Natl. Acad. Sci. U. S. A. **116**, 15350 (2019).

[6] A. Kumar and J. Bechhoefer, Nature **584**, 64–68 (2020).

[7] N. Vadakkayil and S.K. Das, Phys. Chem. Chem. Phys. **23**, 19 (2021).

[8] R.B. Potts, Proc. Camb. Phil Soc. **48**(1), 106 (1952).

[9] T. Kihara, Y. Midzuno, and T. Shizume, J. Phys. Soc. Japan **9**, 681 (1954).

[10] R.J. Baxter, J. Phys. C: Solid State Phys. **6** L445 (1973).

[11] F.Y. Wu, Rev. Mod. Phys. **54**, 235 (1982).

[12] K. Binder, J. Stat. Phys. **24**, pp. 69-86 (1981).

[13] S. Fan and F. Zhong, Phys. Rev. E **76**, 041141 (2007).

[14] B. Berche, P. Butera, W. Janke, and L. Shchur, arXiv:0809.5045 (2008).

[15] A.J. Bray, Adv. Phys. **51**, 481 (2002).

[16] *Kinetics of Phase transition*, edited by S. Puri and V. Wadhawan (CRC Press, Boca Raton, 2009).

[17] K. Kaski, J. Nieminen, and J.D. Gunton, Phys. Rev. B **31**, 2998 (1985).

[18] D.P. Landau and K. Binder, *A Guide to Monte Carlo Simulations in Statistical Physics* (Cambridge University Press, Cambridge, 2009).

[19] S. Majumder and S.K. Das, Phys. Rev. E **81**, 050102 (2010).

[20] S. Majumder and S.K. Das, Phys. Rev. E **84**, 021110 (2011).

[21] S.K. Das and S. Chakraborty, Eur. Phys. J. Spec. Top. **226**, 765 (2017).

[22] M.E. Fisher, Rep. Prog. Phys. **30**, 615 (1967).

[23] M.E. Fisher, in Critical Phenomena, edited by M.S. Green (Academic, London, 1971) p1.

[24] I.G. Enting and A.J. Guttmann Physica A **321** (2003) 90-107.

[25] H.E. Stanley, *Introduction to Phase Transitions and Critical Phenomena* (Clarendon Press, Oxford, 1971).

[26] N. Goldenfeld, *Lectures on Phase Transitions and the Renormalization Group* (West view press, 1992).

[27] T. Ohta, D. Jasnow, and K. Kawasaki, Phys. Rev. Lett. **49**, 1223 (1982).

[28] C. Yeung and D. Jasnow Phys. Rev. B **42**, 10523 (1990).

[29] S.M. Allen and J.W. Cahn, Acta Metall. **27**, 1085 (1979).

[30] T. Vicsek, M. Swesinger, and M. Matsnshita, *Fractals in Natural Sciences* (World scientific, Singapore, 1994).

[31] J. Midya and S.K. Das, Phys. Rev. Lett. **118**, 165701 (2017).

[32] S. Paul, A. Bera, and S.K. Das, Soft Matter **17**, 645 (2021).

[33] K. Kaski, J. Nieminen, and J.D. Gunton Phys. Rev. B **31**, 2998 (1985).

[34] R.E. Blundell and A.J. Bray, Phys. Rev. E **49**, 4925 (1994).

[35] G.S. Grest, M.P. Anderson, and D.J. Srolovitz, Phys. Rev. B **38**, 4752 (1988).

[36] U. Zweck and M. Leitner, Phys. Rev. B **104**, 094101 (2021).

[37] N. Vadakkayil, S. Chakraborty, and S.K. Das, J. Chem. Phys. **150**, 054702 (2019).

[38] J. Olejarz, P.L. Krapivsky, and S. Redner, Phys. Rev. E **83**, 030104(R) (2011).

[39] J. Olejarz, P.L. Krapivsky, and S. Redner, J. Stat. Mech. P06018 (2013).

[40] F. Chippari, L.F. Cugliandolo, and M. Picco, J. Stat. Mech. 093201 (2021).